# Imaginary Scators Quadratic Mapping In 1+2D Dynamic Space

M. Fernández-Guasti[a,*]

[a]*Lab. de Óptica Cuántica, Depto. de Física, Universidad Autónoma Metropolitana - Iztapalapa, C.P. 09340, Ciudad de México, A.P. 55-534, MEXICO.*

---

## Abstract

The elliptic scator algebra quadratic iteration is evaluated in 1+2 dimensions in dynamic space. There exists a non divergent $K$ set in the scator three dimensional space with a highly complex boundary $J = \partial K$. Two and three dimensional renderings of the sets in dynamic space are published for the first time. The sets exhibit a rich fractal boundary in all three directions. Some of the salient features of the sets can be described in terms of square nilpotent iterations. The Julia and filled in Julia sets are identically reproduced at two perpendicular planes where only one non-vanishing hypercomplex director component is present. The fixed points of $K$ in $\mathbb{S}^{1+2}$ with real constant $c$, can be obtained from the roots of a scator quadratic polynomial equation. In $\mathbb{S}^{1+2}$ there can be, in addition to the usual complex roots, hypercomplex roots that give rise to four additional fixed points. The inverse orbits of the hypercomplex roots reveal a rich complex structure, that allow for the evaluation of an infinite set of points in $\partial K$. The $\partial K$ set of the origin is equal to the unit magnitude scator surface, named a cusphere. The $J$ set exhibits self similar structures in 3D at different scales, typical of fractal phenomena. The ix set, is the three dimensional equivalent of the M-set in three dimensions. It is conjectured that the ix-set with some restrictions, is the set of parameters where the $J$ set is connected.

*Keywords:* Hyper-complex numbers, Imaginary scators, Quadratic iteration, Julia set, Discrete dynamical systems

---

## 1. Introduction

The iterated quadratic mapping in the imaginary scator set, produces a rich and complex structure in parameter three dimensional space [1]. In contrast, other algebraic structures with dimension higher than two, such as quaternions, produce a disappointing surface of revolution of the M-set in three dimensions [2,

---

3]. There have been other efforts to extend two dimensional fractal structures to three dimensions such as ternary algebra [4], triplex algebra [5, 6] and variations of them [7]. Visualizations of these sets, in particular quasi-Fuschian fractals [8] and the mandelbulb, have received wide public exposure [9, 10].

In this communication, the three dimensional product and addition operations of imaginary scator algebra are invoked to evaluate the quadratic mapping in dynamic space. Scator algebra is a finite dimensional algebra over the reals with a multiplicative identity, thus fulfilling the hypercomplex algebra Kantor and Solodovnikov criteria except for the distributivity of the product over addition [11]. Scator elements can thus be viewed as hypercomplex numbers in $1 + n$ dimensions if the distributivity condition is relaxed. For $n = 2$, many of the singular properties of this algebra are already present. The scator product is commutative and all elements except zero and infinity have an inverse. Nonetheless, scator algebra is no longer a division algebra because it has zero products of non zero factors. The scator product is associative in the multiplicative representation but not in the additive representation. The algebra is endowed with a second order involution. This feature can be used to establish an order parameter. These peculiarities do not prevent the scator number system from generating consistent iterated quadratic mappings with a rich fractal structure in parameter space [1]. Two theorems are now available that allow relevant progress in the understanding of the scator dynamical system. The Victoria theorem and its concomitant equation, is a generalization of the de Moivre theorem to $1 + n$ dimensional scator space [12]. The roots of scator numbers can be evaluated from a modified version of this theorem [13, 14]. Properties of forward and backward orbits can then be evaluated relying on various forms of these propositions. The second order polynomial equation with real coefficients has been solved in $1 + 2$ dimensional scator space [15]. This result permits the evaluation of fixed points for Julia sets with real constant $c$, thereby obtaining the attractor of the filled in Julia set as well as points on the Julia set. A consequence of these two results is that an infinite number of points in the Julia (boundary) set can be obtained from the fixed point hypercomplex roots.

Scator algebra also produces remarkable iterated quadratic mappings in dynamic space. This is the subject matter of the present communication: In section 2, the essentials of imaginary scator algebra in 1+2 dimensions are presented. The scator quadratic mapping is described in section 3. Three dimensional analogues of the Julia and filled in Julia sets are presented in this section. 2D and 3D renderings illustrate some of the main features of these sets. Square nilpotent points are discussed in subsection 3.2. The fingerprint of the origin is shown in subsection 3.3. Fixed points in scator dynamic space are described in section 4; hypercomplex roots produce extra fixed points with very interesting properties that coexist with the real or imaginary fixed points. Inverse orbits are discussed in section 5, for appropriate parameters, the existence of four additional hypercomplex roots enhances the possibilities and dynamics of the inverse orbits. It also permits the evaluation of new sets of points in the boundary set. Self similar objects within the $K$ set are set forth in section 6. An example is expounded in section 7, where the $K$ set exhibits a Cantor dust structure.

Section 8 is dedicated to two conjectures, given the difficulties encountered to establish formal proofs that necessarily require holomorphy. Conclusions are drawn in the last section.

## 2. Imaginary scators

In the additive representation, scator elements in 1+2 dimensions are written as the sum of three components,

$$\overset{o}{\varphi} = s + x\,\check{\mathbf{e}}_x + y\,\check{\mathbf{e}}_y, \tag{1}$$

where $s, x, y \in \mathbb{R}$ and $\check{\mathbf{e}}_x, \check{\mathbf{e}}_y \notin \mathbb{R}$. The first component is the *scalar component*, while subsequent components are named *director components* [16]. Scator elements are decorated with an oval placed overhead[1]. *Addition* of scators is defined by the sum of coefficients in each component $\overset{o}{\alpha} + \overset{o}{\beta} = (a_0 + a_x\check{\mathbf{e}}_x + a_y\check{\mathbf{e}}_y) + (b_0 + b_x\check{\mathbf{e}}_x + b_y\check{\mathbf{e}}_y) = (a_0 + b_0) + (a_x + b_x)\,\check{\mathbf{e}}_x + (a_y + b_y)\,\check{\mathbf{e}}_y$. Scator numbers satisfy commutative group properties under addition in $\mathbb{R}^{1+2}$.

**Definition 2.1.** The *extended scator product* $\overset{o}{\alpha}\overset{o}{\beta}$ of two scators, $\overset{o}{\alpha} = a_0 + a_x\,\check{\mathbf{e}}_x + a_y\,\check{\mathbf{e}}_y$ and $\overset{o}{\beta} = b_0 + b_x\,\check{\mathbf{e}}_x + b_y\,\check{\mathbf{e}}_y$ is,

$$\overset{o}{\alpha}\overset{o}{\beta} = a_0 b_0 \left(1 - \frac{a_x b_x}{a_0 b_0}\right)\left(1 - \frac{a_y b_y}{a_0 b_0}\right) + a_0 b_0 \left(1 - \frac{a_y b_y}{a_0 b_0}\right)\left(\frac{a_x}{a_0} + \frac{b_x}{b_0}\right)\check{\mathbf{e}}_x$$
$$+ a_0 b_0 \left(1 - \frac{a_x b_x}{a_0 b_0}\right)\left(\frac{a_y}{a_0} + \frac{b_y}{b_0}\right)\check{\mathbf{e}}_y. \tag{2}$$

If there are coefficients equal to zero in the scator factors, the director coefficients limits should be taken prior to the scalar coefficients limit.

The scator product is usually defined in the $\mathbb{S}^{1+2}$ set, where infinity is avoided. The extended scator product allows for divergent products, thereby allowing for an attractor at infinity. The scator product is commonly separated in three distinct cases depending on whether the scalar component vanishes or not. It has been shown that all three possible cases can be obtained through a continuous limiting process of Definition 2.1 in $\mathbb{S}^{1+2}$ [17].

**Example 2.2.** If $a_x = b_x = 0$,

$$\lim_{a_x \to 0, b_x \to 0,} \left(\overset{o}{\alpha}\overset{o}{\beta}\right) = (a_0 b_0 - a_y b_y) + (a_y b_0 + a_0 b_y)\,\check{\mathbf{e}}_y.$$

The usual complex product in $\mathbb{C}$ is recovered. The imaginary unit is $\check{\mathbf{e}}_y$. An analogous result is obtained if $a_y = b_y = 0$, but the imaginary unit is then $\check{\mathbf{e}}_x$.

In the following four examples, all $\overset{o}{\beta}$ components are considered different from zero, $b_0, b_x, b_y \neq 0$.

---

[1] \overset{o} in LATEX lore

**Example 2.3.** The limit $a_0 \to 0$ if $a_x a_y \neq 0$, gives divergent coefficients in all three components,

$$\lim_{a_0 \to 0} \left( \overset{o}{\alpha} \overset{o}{\beta} \right) = \infty + \infty \, \check{\mathbf{e}}_x + \infty \, \check{\mathbf{e}}_y.$$

There are then scator factors with finite coefficients whose product admits infinite coefficients.

**Example 2.4.** If $a_0 = 0$ and $a_x = 0$. The director coefficient limit should be taken first, thus

$$\lim_{a_x \to 0} \left( \overset{o}{\alpha} \overset{o}{\beta} \right) = (a_0 b_0 - a_y b_y) + (a_0 b_0 - a_y b_y) \left( \frac{b_x}{b_0} \right) \check{\mathbf{e}}_x + (a_y b_0 + a_0 b_y) \check{\mathbf{e}}_y;$$

Thereafter, the scalar component limit is evaluated

$$\lim_{a_0 \to 0} \left( \lim_{a_x \to 0} \left( \overset{o}{\alpha} \overset{o}{\beta} \right) \right) = -a_y b_y - a_y b_y \frac{b_x}{b_0} \check{\mathbf{e}}_x + a_y b_0 \check{\mathbf{e}}_y. \tag{3}$$

**Example 2.5.** If one factor has vanishing director coefficients $\overset{o}{\alpha} = a_0 + 0 \, \check{\mathbf{e}}_x + 0 \, \check{\mathbf{e}}_y = a_0$,

$$\overset{o}{\alpha} \overset{o}{\beta} = a_0 \overset{o}{\beta} = a_0 b_0 + a_0 b_x \check{\mathbf{e}}_x + a_0 b_y \check{\mathbf{e}}_y.$$

The $a_0$ component produces a scaling of all the $\overset{o}{\beta}$ scator components. Hence it is rightly named, the scalar component of the scator. $\overset{o}{1} = 1 + 0 \, \check{\mathbf{e}}_x + 0 \, \check{\mathbf{e}}_y = 1$ is the multiplicative neutral.

**Example 2.6.** If $a_x b_x = a_y b_y = a_0 b_0$, then $\overset{o}{\alpha} \overset{o}{\beta} = 0 + 0 \, \check{\mathbf{e}}_x + 0 \, \check{\mathbf{e}}_y$, the scator product is zero. Thus, there exist zero products of non zero factors.

## 2.1. Multiplicative representation of scators

The multiplicative representation of scators is analogous to the polar representation of complex numbers in 1+1 dimensions,

$$\overset{o}{\varphi} = \varphi_0 e^{\varphi_x \, \check{\mathbf{e}}_x} e^{\varphi_y \, \check{\mathbf{e}}_y}, \tag{4}$$

where $e$ is the complex exponential function. $\varphi_0$ is the scator magnitude also named the multiplicative scalar, $\varphi_x$ is the angle of the scator projection between $s$ and the $\check{\mathbf{e}}_x$ axes, $\varphi_y$ is the angle of the projection between $s$ and the $\check{\mathbf{e}}_y$ axes. In the multiplicative representation, the product of two scators is evaluated by performing the product of the magnitudes and the addition of the multiplicative director coefficients with the same director unit [12],

$$\overset{o}{\alpha} \overset{o}{\beta} = \left( \alpha_0 e^{\alpha_x \check{\mathbf{e}}_x} e^{\alpha_y \check{\mathbf{e}}_y} \right) \left( \beta_0 e^{\beta_x \check{\mathbf{e}}_x} e^{\beta_y \check{\mathbf{e}}_y} \right) = \alpha_0 \beta_0 e^{(\alpha_x + \beta_x) \check{\mathbf{e}}_x} e^{(\alpha_y + \beta_y) \check{\mathbf{e}}_y}. \tag{5}$$

The multiplicative scator components having the same director unit $\check{\mathbf{e}}_x$ or $\check{\mathbf{e}}_y$, satisfy the addition theorem for exponents. However, the addition theorem for

exponents does not hold for scators with different director units, i.e. $e^{\varphi_x\,\check{\mathbf{e}}_x}e^{\varphi_y\,\check{\mathbf{e}}_y} \neq e^{\varphi_x\,\check{\mathbf{e}}_x+\varphi_y\,\check{\mathbf{e}}_y}$.

The additive (1) and multiplicative (4) representations of scators are related by

$$\overset{o}{\varphi} = \varphi_0 e^{\varphi_x\,\check{\mathbf{e}}_x}e^{\varphi_y\,\check{\mathbf{e}}_y} = s + x\,\check{\mathbf{e}}_x + y\,\check{\mathbf{e}}_y$$
$$= \varphi_0 \cos\varphi_x \cos\varphi_y + \varphi_0 \cos\varphi_y \sin\varphi_x\,\check{\mathbf{e}}_x + \varphi_0 \cos\varphi_x \sin\varphi_y\,\check{\mathbf{e}}_y. \quad (6)$$

From this expression, it follows that if $s = \varphi_0 \cos\varphi_x \cos\varphi_y = 0$, then $\overset{o}{\varphi} = 0$ or $\overset{o}{\varphi}$ has only one non vanishing director component. Furthermore, if the two director components do not vanish, $\varphi_0 \cos\varphi_y \sin\varphi_x \neq 0$ and $\varphi_0 \cos\varphi_x \sin\varphi_y \neq 0$, then the scalar component is necessarily also different from zero.

**Definition 2.7.** The *scator set* $\mathbb{S}^{1+2} \subset \mathbb{R}^3$, is the subspace where the scalar component is not zero if the two director components are different from zero,

$$\mathbb{S}^{1+2} = \left\{ \overset{o}{\varphi} = s + x\,\check{\mathbf{e}}_x + y\,\check{\mathbf{e}}_y,\ s,x,y \in \mathbb{R} : s \neq 0 \text{ if } x,y \neq 0 \right\}. \quad (7)$$

The $\mathbb{S}^{1+2}$ set avoids divergent products (like the one in Example 2.3). This set was labeled with the letter $\mathbb{E}$ in some of the earlier manuscripts.

*Remark* 2.8. The scator additive and multiplicative representations are equivalent in the $\mathbb{S}^{1+2}$ scator set, except for the kernel of the transformation.

### 2.2. Magnitude

The conjugate of the scator is given by the negative of the director components, leaving the scalar component unchanged in either representation. In the additive representation, $\overset{o}{\varphi}{}^* = s - x\check{\mathbf{e}}_x - y\check{\mathbf{e}}_y$ is the conjugate of $\overset{o}{\varphi} = s + x\check{\mathbf{e}}_x + y\check{\mathbf{e}}_y$. In the multiplicative representation, $\overset{o}{\varphi}{}^* = \varphi_0\, e^{-\varphi_x\,\check{\mathbf{e}}_x}e^{-\varphi_y\,\check{\mathbf{e}}_y}$ is the conjugate of $\overset{o}{\varphi} = \varphi_0 e^{\varphi_x\,\check{\mathbf{e}}_x}e^{\varphi_y\,\check{\mathbf{e}}_y}$. The magnitude of a scator is equal to the positive square root of the scator times its conjugate $\|\overset{o}{\varphi}\| = \sqrt{\overset{o}{\varphi}\overset{o}{\varphi}{}^*}$. In the multiplicative representation from (5), $\|\overset{o}{\varphi}\| = \varphi_0$, the multiplicative scalar is thus the scator magnitude. In the additive representation, the square magnitude is

$$\|\overset{o}{\varphi}\|^2 = \overset{o}{\varphi}\overset{o}{\varphi}{}^* = s^2 \left(1 + \frac{x^2}{s^2}\right)\left(1 + \frac{y^2}{s^2}\right). \quad (8)$$

The multiplicative inverse, from (8) is $\overset{o}{\varphi}{}^{-1} = \overset{o}{\varphi}{}^* \|\overset{o}{\varphi}\|^{-2}$ and in terms of additive variables, the inverse is

$$\overset{o}{\varphi}{}^{-1} = s^{-2}\left(1 + \frac{x^2}{s^2}\right)^{-1}\left(1 + \frac{y^2}{s^2}\right)^{-1}\overset{o}{\varphi}{}^*. \quad (9)$$

A scator is invertible except if all additive components are zero or if $s = 0$ when $xy \neq 0$.

**Definition 2.9.** The *extended scator set* $\bar{\mathbb{S}}^{1+2} = \mathbb{R}^3 \cup \{\infty\}$, allows for all three scator coefficients to be in the reals plus infinity

$$\bar{\mathbb{S}}^{1+2} = \left\{ \overset{o}{\varphi} = s + x\,\check{\mathbf{e}}_x + y\,\check{\mathbf{e}}_y, \ s, x, y \in \mathbb{R} \cup \{\infty\} \right\}, \tag{10}$$

The points at infinity are attained if any of the scator components becomes infinite, i.e. $s \to \infty$ and/or $x \to \infty$ and/or $y \to \infty$. The magnitude of these points is infinite. Although the set of points with zero scalar component $s = 0$ and two nonvanishing director components $xy \neq 0$ have finite coefficients, their magnitude is also infinite. Elements in $\bar{\mathbb{S}}^{1+2} \setminus \mathbb{S}^{1+2}$ have divergent magnitude. This state of affairs has led to the concept of *divergent vicinity* whenever the zero scator is involved [1]. The element $0 + 0\,\check{\mathbf{e}}_x + 0\,\check{\mathbf{e}}_y$ has a divergent vicinity since the magnitude of $0 + \delta x\,\check{\mathbf{e}}_x + \delta y\,\check{\mathbf{e}}_y$ is infinite if $\delta x, \delta y \neq 0$. The scator magnitude does not diverge in $\mathbb{S}^{1+2}$.

*Remark* 2.10. There exists a scator multiplicative representation for elements in the $\mathbb{S}^{1+2}$ scator set but not in $\bar{\mathbb{S}}^{1+2} \setminus \mathbb{S}^{1+2}$.

Let us mention two propositions that will be useful in the coming sections:

**Lemma 2.11** (Fernandez-Guasti, 2016). *The only non trivial square nilpotent elements $\overset{o}{\varphi}^2 = 0 + 0\,\check{\mathbf{e}}_x + 0\,\check{\mathbf{e}}_y$ in 1+2 dimensional imaginary scator algebra are elements whose three components have equal absolute value, $\overset{o}{\varphi} = \pm g \pm g\,\check{\mathbf{e}}_x \pm g\,\check{\mathbf{e}}_y$.*

**Corollary 2.12** (Fernandez-Guasti, 2016). *The square of an invertible element is invertible if it is not square nilpotent.*

## 3. Iterated quadratic mapping

Consider a function $\overset{o}{f} : \bar{\mathbb{S}}^{1+2} \to \bar{\mathbb{S}}^{1+2}$ to be a scator function of scator variable.

**Definition 3.1.** The non divergent set $K(\overset{o}{f})$ in dynamic space for imaginary scators in 1+2 dimensions is given by

$$K(\overset{o}{f}) = \left\{ \overset{o}{\varphi} \in \bar{\mathbb{S}}^{1+2} : \forall m \in \mathbb{N}, \left\| \overset{o}{f}^m (\overset{o}{\varphi}) \right\| \nrightarrow \infty \right\}, \tag{11}$$

where $\overset{o}{f}^m$ denotes the *m-fold composition* $\overset{o}{f}^m = \overset{o}{f}(\overset{o}{f}(\overset{o}{f} \cdots))$ of the function $\overset{o}{f} \in \mathbb{S}^{1+2}$.

$K(\overset{o}{f})$ is a three dimensional generalization of the filled in Julia set. In this generalization, the Julia set is again defined as the boundary of the filled in Julia set $J(\overset{o}{f}) = \partial K(\overset{o}{f})$. This boundary is now embedded in an $\bar{\mathbb{S}}^{1+2}$ three dimensional space. The filled in $K(\overset{o}{f})$ set has been defined in terms of a non divergent condition rather than a bounded one. This will be relevant, as we

shall see further down, because nilpotent points can have very large magnitude but are nonetheless in the $K$ set.

The square of a scator $\overset{o}{\varphi} = s + x\check{\mathbf{e}}_x + y\check{\mathbf{e}}_y$ is obtained from the product of two equal scators, $\overset{o}{\varphi}^2 = (s + x\check{\mathbf{e}}_x + y\check{\mathbf{e}}_y)^2$. From Eq. (2)

$$\overset{o}{\varphi}^2 = s^2\left(1 - \frac{x^2}{s^2}\right)\left(1 - \frac{y^2}{s^2}\right) + 2sx\left(1 - \frac{y^2}{s^2}\right)\check{\mathbf{e}}_x + 2sy\left(1 - \frac{x^2}{s^2}\right)\check{\mathbf{e}}_y. \quad (12)$$

The square function mapping $q : \mathbb{S}^{1+n} \to \mathbb{S}^{1+n}, \overset{o}{\varphi} \mapsto \overset{o}{\varphi}^2$ satisfies $q(\lambda\overset{o}{\varphi}) = \lambda^2 q(\overset{o}{\varphi})$, $\lambda \in \mathbb{R}$. In the multiplicative representation, the square of a scator is

$$\overset{o}{\varphi}^2 = \varphi_0^2\, e^{2\varphi_x\check{\mathbf{e}}_x} e^{2\varphi_y\check{\mathbf{e}}_y}. \quad (13)$$

Consider the family of maps $\overset{o}{f}_c : \overset{o}{\varphi} \mapsto \overset{o}{\varphi}^2 + \overset{o}{c}$ from $\bar{\mathbb{S}}^{1+2}$ to $\bar{\mathbb{S}}^{1+2}$, where the variable $\overset{o}{\varphi}$ and the constant $\overset{o}{c}$ are scator elements. The iteration procedure in dynamic space is obtained by fixing an initial constant $\overset{o}{c}$ and evaluating, for each point $\overset{o}{\varphi}$ in the scator space, the quadratic recurrence relationship

$$\overset{o}{\varphi}_{m+1} = \overset{o}{\varphi}_m^2 + \overset{o}{c}. \quad (14)$$

Non divergent points obtained for an arbitrary number of iterations comprise the $K$ set in $\bar{\mathbb{S}}^{1+2}$. In terms of the additive coefficients, for each point $\overset{o}{\varphi}_1 = s_1 + x_1\check{\mathbf{e}}_x + y_1\check{\mathbf{e}}_y$ and $\overset{o}{c} = c_s + c_x\check{\mathbf{e}}_x + c_y\check{\mathbf{e}}_y$, the quadratic iteration recurrence relationship for the scalar component is

$$s_{m+1} = s_m^2\left(1 - \frac{x_m^2}{s_m^2}\right)\left(1 - \frac{y_m^2}{s_m^2}\right) + c_s \quad (15a)$$

and for the director components,

$$x_{m+1} = 2s_m x_m\left(1 - \frac{y_m^2}{s_m^2}\right) + c_x, \quad (15b)$$

$$y_{m+1} = 2s_m y_m\left(1 - \frac{x_m^2}{s_m^2}\right) + c_y. \quad (15c)$$

The iteration (15a)-(15c) has been implemented in the Mandelbulber (version 2.20-dev) three dimensional fractal visualization program. Very intricate surfaces are obtained that are difficult to handle by ray tracing programs. The processing power required to generate 3D fractals is greatly increased compared with 2D renderings. It is necessary to extend the two dimensional image grid to three dimensional space. An image with $10^3$ pixels resolution in each axis, requires $10^9$ voxels (1000 million points!). Thus, the iteration of a much larger set of points is required to begin with. Thereafter, computer ray tracing is necessary to establish the observer point of view, with the concomitant occlusion of interior points or points that lie behind a particular surface from the observer
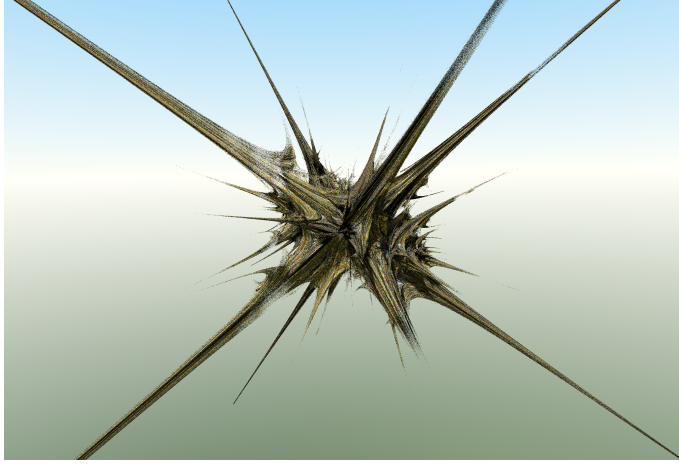
Figure 1: Non divergent set in 3D dynamic scator space, $K\big(\overset{o}{\varphi}{}^{2} + \overset{o}{\varphi}_c\big) \in \mathbb{S}^{1+2}$ of the $\overset{o}{c} = -0.5 + 0\,\check{\mathbf{e}}_x + 0.5\,\check{\mathbf{e}}_y$ hypercomplex point, seen from $\overset{o}{v} = 3 - 8\,\check{\mathbf{e}}_x + 1\,\check{\mathbf{e}}_y$. Image generated with the 'Mandelbulber' rendering program.

point of view. The capability of using parallel GPU processing using OpenCL has greatly enhanced the rendering velocity.

Two dimensional renderings of the 3D $K\big(\overset{o}{f}_c\big)$ set can also be made at a particular 2D plane with standard plots. For example, the set in the $(s, \check{\mathbf{e}}_y)$ plane at a constant $x_0\check{\mathbf{e}}_x$ value is obtained by evaluating the (15a)-(15c) triad for $s + x_0\check{\mathbf{e}}_x + y\check{\mathbf{e}}_y$, for all $s, y$ values. Inclined planes can also be rendered if a condition of the form $x = my$, where $m$ is constant, is imposed. Notice that in these cases, the plane under consideration has no breath, i.e. it is fixed to a single value. In contrast, 3D renderings require voxels, that is 3D tiny boxes; in this case, a plane can be approximated only to within the thickness of the minimum voxel size.

*3.1. Non divergent set in dynamic space for $\overset{o}{c} = -0.5 + 0\,\check{\mathbf{e}}_x + 0.5\,\check{\mathbf{e}}_y$*

Consider, as an initial example, the quadratic iteration non divergent set in dynamic $\mathbb{S}^{1+2}$ scator space $K\big(\overset{o}{\varphi}{}^{2} + \overset{o}{c}\big)$ for the hypercomplex point $\overset{o}{c} = -0.5 + 0\,\check{\mathbf{e}}_x + 0.5\,\check{\mathbf{e}}_y$. The rendered set, observed from $\overset{o}{v} = 3 - 8\,\check{\mathbf{e}}_x + 1\,\check{\mathbf{e}}_y$, is shown in figure 1. This set is equivalent to the filled in Julia set in the complex plane $K\big(z^2 + z_c\big) \in \mathbb{C}$, $z_c = -0.5 + 0.5i$ but extended to three dimensional space. The fractal nature of the surface makes it very difficult to produce an accurate ray tracing reflection due to the boundary roughness.

A close up of the central region is shown in figure 2a. The surface exhibits an intricate pattern of streaks in different directions. There is, so far, hardly any resemblance of this figure with a filled in Julia set. It is possible to limit the rendering to a region in the mandelbulber program. In figure 2b, the set is limited to $0 \le x \le 10$ region in the $\check{\mathbf{e}}_x$ direction and left in the default $\pm 10$
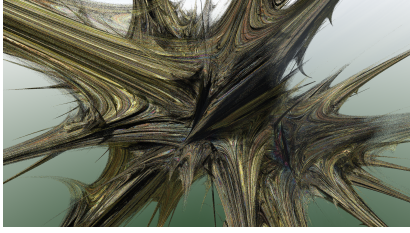
(a) Rendering for values within ±10 in all three variables.
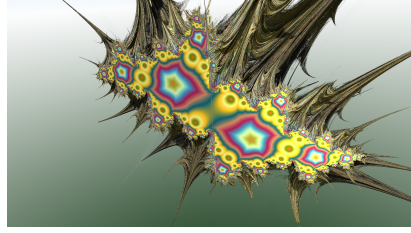
(b) Rendering restricted to the $0 \leq x \leq 10$ region in the $\check{\mathbf{e}}_x$ axis.

Figure 2: $K\!\left(\overset{o}{\varphi}{}^{2} + \overset{o}{c}\right)$ closer detail of the $\overset{o}{c} = -0.5 + 0\,\check{\mathbf{e}}_x + 0.5\,\check{\mathbf{e}}_y$ hypercomplex point, seen from $\overset{o}{v} = 0.75 - 2\,\check{\mathbf{e}}_x + 1\,\check{\mathbf{e}}_y$.

limits in the scalar and $\check{\mathbf{e}}_y$ axes. The set inside colouring, established by the programmers, is determined by the value at the end of the orbit trap iterations. The surface cut at $x = 0$ begins to look a bit more familiar.

If the observation point is located on the $\check{\mathbf{e}}_x$ axis, figure 3a is obtained and if the rendering is further restricted to a region very close to the $x = 0$ plane, figure 3b is obtained. In a 3D rendering, the voxels have finite size in all three directions, in fact, they are usually tiny cubes. This means that the $x = 0$ plane cannot be chosen with zero breath. It has to encompass a finite albeit small depth. Some kinks, particularly evident close to the $s = 0$ line, are a consequence of this finite depth. For comparison, a filled in Julia set $K\,(z_c)$ for $z_c = -0.5 + 0.5i$ in the complex plane is shown in figure 3c. The two sets are remarkably similar, the irrelevant filled in colouring making for most of the difference. The minor differences, mainly observed close to $s = 0$, but present in the whole frontier when looked in detail, can be attributed to the finite depth of the 3D rendering. To confirm this assertion, the voxel size is estimated to be $6.1 \times 10^{-3}$ per side. The 3D program is then evaluating the $x = 0$ plane with $\pm 3.05 \times 10^{-3}$ resolution. In figure 3d, a 2D rendering at the $\overset{o}{\varphi} = x + 0.003\,\check{\mathbf{e}}_x + y\,\check{\mathbf{e}}_y$ hypercomplex plane is depicted. This set exhibits the kinks absent in the Julia set, but present in the 3D rendering.

### 3.2. Nilpotent elements

Besides the central bundle, there are eight straight long filaments extending from the center up to large coordinate values. There are also smaller spikes that describe hyperbolic like curves. These broad features can be understood in terms of nilpotency. The constant $\overset{o}{c}$ is obtained on the first iteration if the initial point is square nilpotent,

$$\overset{o}{\varphi}_2 = \overset{o}{\varphi}{}^{2}_{nil1} + \overset{o}{c} = \overset{o}{c}.$$
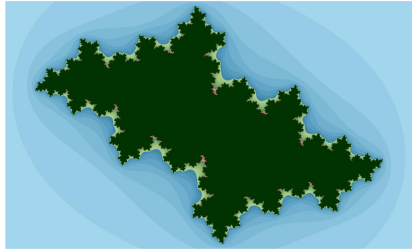
Thereafter, the iterations in dynamic space follow the orbit of the point $\overset{o}{c}$ in parameter space, i.e. $\{\overset{o}{\varphi}_{nil}, \overset{o}{c}, \overset{o}{c}{}^{2} + \overset{o}{c}, \left(\overset{o}{c}{}^{2} + c\right)^{2} + \overset{o}{c}, ...\}$. The quadratic iteration
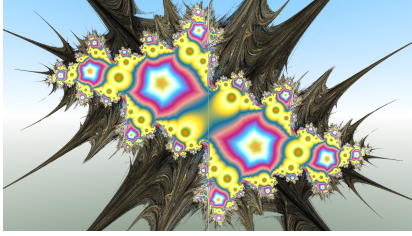
(a) $K\left(\overset{o}{\varphi}^2 + \overset{o}{c}\right)$ seen from $\overset{o}{v} = 0 - 2\,\check{\mathbf{e}}_x + 0\,\check{\mathbf{e}}_y$ restricted to $0 \leq x \leq 10$.
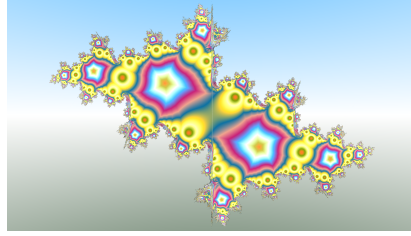


(b) $K\left(\overset{o}{\varphi}^2 + \overset{o}{c}\right)$ seen from $\overset{o}{v} = 0 - 2\,\check{\mathbf{e}}_x + 0\,\check{\mathbf{e}}_y$ but restricted to the minimum voxel size in $x$, $-0.003 \leq x \leq 0.003$.



(c) Familiar filled in Julia set of the $z_c = -0.5 + 0.5i$ point in the complex plane obtained from a standard 2D plot.
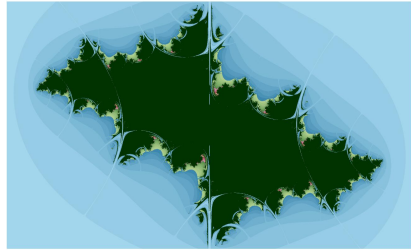


(d) $K\left(\overset{o}{\varphi}^2 + \overset{o}{c}\right)$ evaluated at the plane $\overset{o}{\varphi} = s + 0.003\check{\mathbf{e}}_x + y\check{\mathbf{e}}_y$, with a standard 2D plot.

Figure 3: $K\left(\overset{o}{\varphi}^2 + \overset{o}{c}\right)$ detail of the $\overset{o}{c} = -0.5 + 0\,\check{\mathbf{e}}_x + 0.5\,\check{\mathbf{e}}_y$ hypercomplex point. Comparison of a thin 3D slice seen from the $\check{\mathbf{e}}_x$ direction, the Julia set in the complex plane and a 2D rendering with an offset of 0.003 in the $\check{\mathbf{e}}_x$ hypercomplex plane.

bound set in parameter $\mathbb{S}^{1+2}$ scator space is coined here as the Ix-set[2]. This set has been described in an earlier communication [1]. The Mandelbrot set is a subset of the Ix-set, M $\subset$ Ix if any of the two director components is equal to zero. The sequence $\{\overset{o}{\varphi}_{nil}, \overset{o}{c}, \overset{o}{c}{}^2 + \overset{o}{c}, (\overset{o}{c}{}^2 + c)^2 + \overset{o}{c}, ...\}$ does not diverge if the constant $\overset{o}{c}$ belongs to the Ix-set. The orbit of all nilpotent initial points after the first iteration is the same and is the sequence of $\overset{o}{c}$ in parameter space. If the constant $\overset{o}{c}$ is in the Ix-set, it is a bound point and therefore nilpotent points will be in the $K(\overset{o}{\varphi}{}^2 + \overset{o}{c})$ set. From Lemma 2.11, nilpotent elements have equal absolute value of the scalar and director components. The four $\overset{o}{\varphi} = \overset{o}{\gamma} = \pm g \pm g\check{\mathbf{e}}_x \pm g\check{\mathbf{e}}_y$ straight lines are tilted $\pm 45°$ with respect to the $s, \check{\mathbf{e}}_x$ and $s, \check{\mathbf{e}}_y$ projections. The azimuthal angle with respect to any of the axes is $\arctan\left(\pm\sqrt{2}\right) \approx \pm 54.7°$. The eight main spikes present in the $K(\overset{o}{\varphi}{}^2 + \overset{o}{c})$ sets for $\overset{o}{c} \in$ Ix-set, are due to this nilpotent feature. These spikes extend to arbitrarily large values of $g$.

**Lemma 3.2.** *A point $\overset{o}{\varphi}$ whose $m^{th}$ iteration is square nilpotent belongs to the $K$ set if the constant $\overset{o}{c}$ does not diverge in parameter space.*

*Proof.* For a point that is square nilpotent after $m$ iterations, the $m+1$ iteration is equal to $\overset{o}{c}$, $\overset{o}{\varphi}_m^2 + \overset{o}{c} = \overset{o}{c}$. Thereafter, the sequence is equal to that of $\overset{o}{c}$ in parameter space. The forward orbit is $\{\overset{o}{\varphi}_1, \overset{o}{\varphi}_2, \ldots, \overset{o}{\varphi}_m, \overset{o}{\varphi}_m^2 + \overset{o}{c} = \overset{o}{c}, \overset{o}{c}{}^2 + \overset{o}{c}, ...\}$. Therefore $\overset{o}{\varphi}$ does not diverge in dynamic space if $\overset{o}{c}$ does not diverge in parameter space. $\square$

**Lemma 3.3.** *There is no upper bound for the set of points that are nilpotent upon the $m^{th}$ iteration.*

*Proof.* If $\overset{o}{\varphi}_m$ is square nilpotent, from Lemma 2.11, its additive components must have equal absolute value, $\overset{o}{\varphi}_m = \overset{o}{\gamma} = \pm g \pm g\check{\mathbf{e}}_x \pm g\check{\mathbf{e}}_y$. The magnitude of $\overset{o}{\gamma}$ from (8), is $\left\|\overset{o}{\gamma}\right\| = 2|g|$. The multiplicative angle variables are obtained from the quotient of the directors over the scalar component, $\gamma_x = \gamma_y = \arctan\left(\frac{g}{g}\right) = \frac{\pi}{4}$. The multiplicative representation of the scator $\overset{o}{\gamma}$ is then

$$\overset{o}{\gamma} = 2ge^{\frac{\pi}{4}\check{\mathbf{e}}_x}e^{\frac{\pi}{4}\check{\mathbf{e}}_y}.$$

Consider the constant $\overset{o}{c}$ to be much smaller than any of the $\overset{o}{\varphi}_j$ iterates, so that $\overset{o}{\varphi}_j^2 + \overset{o}{c} \approx \overset{o}{\varphi}_j^2$. Upon each iteration the exponent is doubled, $\overset{o}{\varphi}_m = \overset{o}{\gamma} = \overset{o}{\varphi}_1^{2^m}$. The initial point $\overset{o}{\varphi}_1$ is thus obtained from inversion of this equation

$$\overset{o}{\varphi}_1 = \overset{o}{\varphi}_m^{\frac{1}{2^m}} = \overset{o}{\gamma}^{\frac{1}{2^m}}.$$

---

[2] Ix is pronounced ish, like in lavish.

From the Victoria Theorem in the multiplicative representation [14], the $q^{th}$ root of $\overset{o}{\varphi}$ in $\mathbb{S}^{1+2}$ is

$$\overset{o}{\varphi}{}^{\frac{1}{q}} = \left( \varphi_0 e^{\varphi_x \check{\mathbf{e}}_x} e^{\varphi_y \check{\mathbf{e}}_y} \right)^{\frac{1}{q}}$$

$$= \varphi_0^{\frac{1}{q}} \exp\left[ \frac{1}{q} \left( \varphi_x + 2\pi r_x + \sigma\pi \right) \check{\mathbf{e}}_x \right] \exp\left[ \frac{1}{q} \left( \varphi_y + 2\pi r_y + \sigma\pi \right) \check{\mathbf{e}}_y \right],$$

where $r_x, r_y \in \mathbb{Z}$, from 0 to $q-1$ and $\sigma$ is 0 or 1. In the particular case of $\overset{o}{\gamma}{}^{\frac{1}{2m}}$,

$$\overset{o}{\gamma}{}^{\frac{1}{2m}} = \sqrt[2^m]{2|g|} \exp\left[ \frac{1}{2^m} \left( \frac{\pi}{4} + 2\pi r_x + \sigma\pi \right) \check{\mathbf{e}}_x \right] \exp\left[ \frac{1}{2^m} \left( \frac{\pi}{4} + 2\pi r_y + \sigma\pi \right) \check{\mathbf{e}}_y \right]. \tag{16}$$

The magnitude of this scator is $\left\| \overset{o}{\varphi}_1 \right\| = \left\| \overset{o}{\gamma}{}^{\frac{1}{2m}} \right\| = \sqrt[2^m]{2|g|}$. Since $g$ can be arbitrarily large, the magnitude of the initial point $\overset{o}{\varphi}_1$ does not have an upper bound. $\qquad\square$

**Corollary 3.4.** *The $\frac{x}{s}$ and $\frac{y}{s}$ asymptotes of nilpotent points upon the $m^{th}$ iteration are $\tan\left( \frac{\pi}{2^{m+2}} \bmod \frac{\pi}{2^m} \right)$.*

*Proof.* From the multiplicative to additive representation (6) of the roots given by (16),

$$\overset{o}{\varphi}_1 = s + x\,\check{\mathbf{e}}_x + y\,\check{\mathbf{e}}_y = \overset{o}{\gamma}{}^{\frac{1}{2m}}$$

$$= \sqrt[2^m]{2|g|} \cos\left( \frac{\frac{\pi}{4} + 2\pi r_x + \sigma\pi}{2^m} \right) \cos\left( \frac{\frac{\pi}{4} + 2\pi r_y + \sigma\pi}{2^m} \right)$$

$$+ \sqrt[2^m]{2|g|} \cos\left( \frac{\frac{\pi}{4} + 2\pi r_y + \sigma\pi}{2^m} \right) \sin\left( \frac{\frac{\pi}{4} + 2\pi r_x + \sigma\pi}{2^m} \right) \check{\mathbf{e}}_x$$

$$+ \sqrt[2^m]{2|g|} \cos\left( \frac{\frac{\pi}{4} + 2\pi r_x + \sigma\pi}{2^m} \right) \sin\left( \frac{\frac{\pi}{4} + 2\pi r_y + \sigma\pi}{2^m} \right) \check{\mathbf{e}}_y. \tag{17}$$

The quotient of the directors over the scalar component are

$$\frac{x}{s} = \tan\left( \frac{\pi}{2^{m+2}} \pm \frac{\pi}{2^m} r_x \right), \quad \frac{y}{s} = \tan\left( \frac{\pi}{2^{m+2}} \pm \frac{\pi}{2^m} r_y \right).$$

$$\square$$

The $\overset{o}{\varphi}_j^2 + \overset{o}{c} \approx \overset{o}{\varphi}_j^2$ approximation is extremely crude. A richer structure is obtained if the constant is not neglected, although the analytic expressions become rather awkward upon iteration. Consider points that are nilpotent on the second iteration, $\left( \overset{o}{\varphi}_1^2 + \overset{o}{c} \right)^2 = 0$, then $\left( \overset{o}{\varphi}_1^2 + \overset{o}{c} \right)_{nil}$ is square nilpotent and thus the absolute value of its coefficients must be equal,

$$\overset{o}{\varphi}_2 = \left( \overset{o}{\varphi}_1^2 + \overset{o}{c} \right)_{nil} = \overset{o}{\gamma} = \pm g \pm g\check{\mathbf{e}}_x \pm g\check{\mathbf{e}}_y.$$

The forward orbit for these points is $\{\overset{o}{\varphi}_1, \left(\overset{o}{\varphi}{}_1^2 + \overset{o}{c}\right)_{nil}, \overset{o}{c}, \overset{o}{c}{}^2 + \overset{o}{c}, \left(\overset{o}{c}{}^2 + c\right)^2 + \overset{o}{c}, ...\}$.
For $\overset{o}{c} = c_0 + c_x \check{\mathbf{e}}_x + c_y \check{\mathbf{e}}_y$, the initial point $\overset{o}{\varphi}_1$ has to satisfy

$$\overset{o}{\varphi}_1 = \sqrt{\overset{o}{\gamma} - \overset{o}{c}} = \sqrt{(\pm g - c_0) + (\pm g - c_x)\,\check{\mathbf{e}}_x + (\pm g - c_y)\,\check{\mathbf{e}}_y}.$$

Returning momentarily to the first order approximation, in the limit when $g \gg c_0, c_x, c_y$, $\overset{o}{\varphi}{}_1^2 + \overset{o}{c} \approx \overset{o}{\varphi}{}_1^2 = g + g\check{\mathbf{e}}_x + g\check{\mathbf{e}}_y$, the roots of a square nilpotent element $\sqrt{\pm g \pm g\check{\mathbf{e}}_x \pm g\check{\mathbf{e}}_y}$ are

$$\overset{o}{\zeta}_{\pm,0} = \pm\frac{\sqrt{|g|}}{2}\left[\left(\sqrt{2}+1\right) \pm \check{\mathbf{e}}_x \pm \check{\mathbf{e}}_y\right], \quad \overset{o}{\zeta}_{\pm,1} = \pm\frac{\sqrt{|g|}}{2}\left[\left(\sqrt{2}-1\right) \mp \check{\mathbf{e}}_x \mp \check{\mathbf{e}}_y\right].$$

There are thus spikes at

$$\arctan\left(\pm\frac{1}{\sqrt{2}+1}\right) = \pm\frac{\pi}{8} = \pm 22.5°, \text{ and } \arctan\left(\pm\frac{1}{\sqrt{2}-1}\right) = \pm\frac{3\pi}{8} = \pm 67.5°$$

with respect to the $s, \check{\mathbf{e}}_x$ and $s, \check{\mathbf{e}}_y$ projections. These results are equivalent to (17) with $m = 1$, but written in terms of additive variables.

If the constant $\overset{o}{c}$ is a scalar $\overset{o}{c} = c_0$, $(c_x = c_y = 0)$, the points that are square nilpotent on the second iteration are, as shown in the appendix,

$$\overset{o}{\zeta}_{\pm,0} = \frac{1}{2}\sqrt{\frac{1}{|g - c_0|}}\left[\pm\left(\sqrt{2g^2 - 2gc_0 + c_0^2} + (g - c_0)\right) \pm g\,\check{\mathbf{e}}_x \pm g\,\check{\mathbf{e}}_y\right], \quad (18a)$$

and from the $\pi$-pair symmetry,

$$\overset{o}{\zeta}_{\pm,1} = \frac{1}{2}\sqrt{\frac{1}{|g - c_0|}}\left[\pm\left(\sqrt{2g^2 - 2gc_0 + c_0^2} - (g - c_0)\right) \pm g\check{\mathbf{e}}_x \pm g\check{\mathbf{e}}_y\right]. \quad (18b)$$

A plot of these points for $-30 \le g \le 30$ and $\check{\mathbf{e}}_x, \check{\mathbf{e}}_y$ coefficients with equal sign is shown in figure 4. A similar plot tilted at 90° is obtained for $\check{\mathbf{e}}_x, \check{\mathbf{e}}_y$ coefficients with opposite sign. The hyperbolic like curves in figure 4 are qualitatively identified with some of the fibre bundles shapes in the various $K$ sets shown in this work. The plots specifically correspond to nilpotent points on the second iteration of the $K\left(\overset{o}{\varphi}{}^2 - \frac{1}{2}\right)$ set described in subsection 4.1.

### 3.3.  The fingerprint of the origin.

Consider the constant point to be the origin, $\overset{o}{c} = 0 + 0\,\check{\mathbf{e}}_x + 0\,\check{\mathbf{e}}_y$. The quadratic iteration is then

$$\overset{o}{\varphi}_{m+1} = \overset{o}{\varphi}{}_m^2.$$

From the multiplicative to additive representations (6) and the square of a scator in the multiplicative representation (13), the square of a scator is

$$\overset{o}{\varphi}{}^2 = \varphi_0^2\, e^{2\varphi_x\,\check{\mathbf{e}}_x} e^{2\varphi_y\,\check{\mathbf{e}}_y}$$
$$= \varphi_0^2\left[\cos\left(2\varphi_x\right)\cos\left(2\varphi_y\right) + \cos\left(2\varphi_y\right)\sin\left(2\varphi_x\right)\,\check{\mathbf{e}}_x + \cos\left(2\varphi_x\right)\sin\left(2\varphi_y\right)\,\check{\mathbf{e}}_y\right].$$
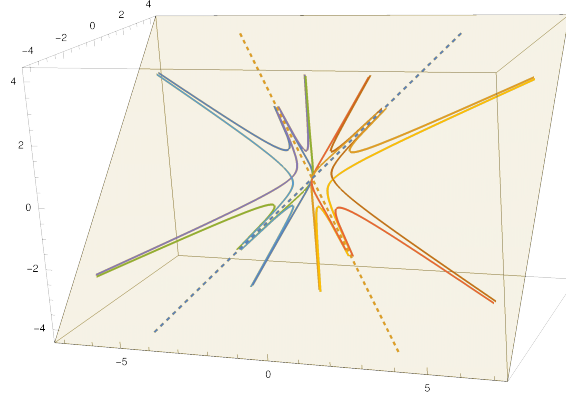
Figure 4: Roots $\overset{o}{\zeta}_{\pm,0}$ and $\overset{o}{\zeta}_{\pm,1}$ for director components with equal signs, $c_0 = -\frac{1}{2}$ in Eqs. (18a) and (18b). These lines correspond to nilpotent points on the second iteration for $-30 \leq g \leq 30$. Nilpotent points on the first iteration are shown with dotted lines.

Its magnitude is $\left\|\overset{o}{\varphi}^2\right\| = \varphi_0^2$. The doubling of angles produces a scator rotation (not an Euclidean rotation) in the $s, \check{\mathbf{e}}_x$ and $s, \check{\mathbf{e}}_y$ planes that does not alter the scator magnitude. A repeated iteration $\overset{o}{\varphi}_{m+1} = \overset{o}{\varphi}_m^2$ will then make the magnitude increase indefinitely for $\left\|\overset{o}{\varphi}\right\| > 1$ and will decrease monotonically for $\left\|\overset{o}{\varphi}\right\| < 1$. The magnitude will only be invariant for unit magnitude scators $\left\|\overset{o}{\varphi}\right\| = 1$. The set for the origin in dynamic space should then be the isometric surface. This is indeed the case, figure 5a shows the 3D rendering of the $J\left(\overset{o}{\varphi}^2\right)$ set for $\overset{o}{c} = 0 + 0\,\check{\mathbf{e}}_x + 0\,\check{\mathbf{e}}_y$. For comparison, the cusphere surface, drawn for unit magnitude from Eq. (6), is shown in figure 5b. The $J\left(\overset{o}{\varphi}^2\right)$ set is compared with the isometric surface rather than $K\left(\overset{o}{\varphi}^2\right)$ because it is the boundary $J = \partial K$ that is actually equal to the cusphere surface.

The $J$ set for the origin in $\mathbb{S}^{1+2}$, is a higher dimensional analogue of its counterpart in the complex plane. In $\mathbb{C}$, the Julia set of the origin is a unit circle, i.e. the constant Euclidean metric in 2D. Recall that the constant scator metric (8) degenerates onto a circle for $x = 0$ or $y = 0$. In $1 + 2D$, the constant scator magnitude departs from the sphere (the 3D Euclidean constant metric). The cusphere is the constant scator magnitude surface for elliptic scators in $\mathbb{S}^{1+2}$ [18].

## 4. Fixed points

**Lemma 4.1.** *The fixed points in $\mathbb{S}^{1+2}$ scator space for the quadratic iteration $\overset{o}{\varphi}_{m+1} = \overset{o}{\varphi}_m^2 + \overset{o}{c}$, provided that the constant $\overset{o}{c} = c + 0\,\check{\mathbf{e}}_x + 0\,\check{\mathbf{e}}_y$ is a scalar are:*
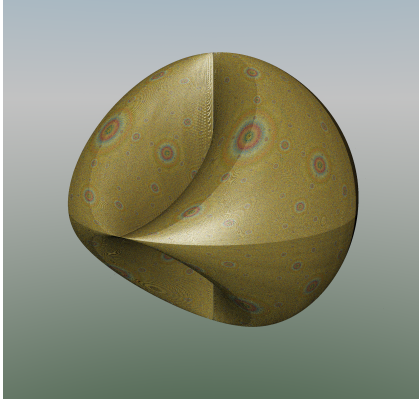
(a) $J(\overset{o}{\varphi}{}^2)$ seen from $\overset{o}{v} = 1.4 - 2.5\,\check{\mathbf{e}}_x + 0.7\,\check{\mathbf{e}}_y$.
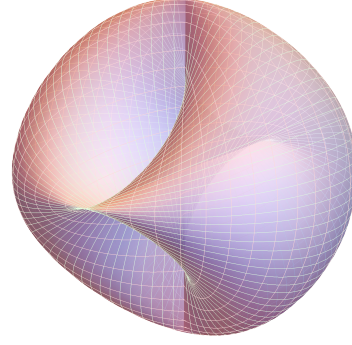


(b) Cusphere drawn from parametric plot of Eq. (6) with $\varphi_0 = 1$

Figure 5: Bound set for the origin $\overset{o}{c} = 0 + 0\,\check{\mathbf{e}}_x + 0\,\check{\mathbf{e}}_y$ and the cusphere rendered from the unit scator magnitude condition, $\|\overset{o}{\varphi}\| = 1$.

If $|4c| > 1$, *(four hypercomplex roots)*

$$\overset{o}{\varphi}_{\mathbb{S}^{1+2}\setminus\mathbb{S}^{1+1}} = \left(c + \frac{1}{4}\right) \pm \frac{1}{4}\sqrt{16c^2 - 1}\,\check{\mathbf{e}}_x \pm \frac{1}{4}\sqrt{16c^2 - 1}\,\check{\mathbf{e}}_y; \qquad (19a)$$

If $4c \leq 1$, *(real roots)*,

$$\overset{o}{\varphi}_{\mathbb{S}^{1+0}} = \frac{1}{2} \pm \frac{1}{2}\sqrt{1 - 4c}; \qquad (19b)$$

If $4c > 1$, *(two copies of the complex like roots)*,

$$\overset{o}{\varphi}_{\mathbb{S}^{1+1}_x} = \frac{1}{2} \pm \frac{1}{2}\sqrt{4c - 1}\,\check{\mathbf{e}}_x, \quad \overset{o}{\varphi}_{\mathbb{S}^{1+1}_y} = \frac{1}{2} \pm \frac{1}{2}\sqrt{4c - 1}\,\check{\mathbf{e}}_y. \qquad (19c)$$

*Proof.* The point $\overset{o}{\varphi}$ is fixed if $\overset{o}{\varphi}_{m+1} = \overset{o}{\varphi}_m$ in the quadratic iteration. The polynomial to be solved is then

$$\overset{o}{\varphi}{}^2 - \overset{o}{\varphi} + c = 0, \qquad (20)$$

where $\overset{o}{\varphi} \in \mathbb{S}^{1+2}$. The scator solutions to this polynomial are given by Theorem 1 in [15]:

**Theorem 4.2** (Fernandez-Guasti, 2021)**.** *The second order polynomial* $a\overset{o}{\varphi}{}^2 + b\overset{o}{\varphi} + c = 0$*, where* $\overset{o}{\varphi} \in \mathbb{S}^{1+2}$ *is an elliptic scator and* $a, b, c \neq 0$ *are real coefficients, has the following roots:*
    *If* $|4ac| > b^2$,

$$\overset{o}{\varphi}_{\mathbb{S}^{1+2}\setminus\mathbb{S}^{1+1}} = -\frac{4ac + b^2}{4ab} \pm \sqrt{\frac{(4ac)^2 - (b^2)^2}{16a^2b^2}}\,\check{\mathbf{e}}_x \pm \sqrt{\frac{(4ac)^2 - (b^2)^2}{16a^2b^2}}\,\check{\mathbf{e}}_y; \qquad (21a)$$

*If $4ac \leq b^2$,*

$$\overset{o}{\varphi}_{\mathbb{S}^{1+0}} = -\frac{b}{2a} \pm \frac{\sqrt{b^2 - 4ac}}{2a}; \qquad (21b)$$

*If $4ac > b^2$,*

$$\overset{o}{\varphi}_{\mathbb{S}^{1+1}_1} = -\frac{b}{2a} \pm \frac{\sqrt{-b^2 + 4ac}}{2a}\check{\mathbf{e}}_x, \quad \overset{o}{\varphi}_{\mathbb{S}^{1+1}_2} = -\frac{b}{2a} \pm \frac{\sqrt{-b^2 + 4ac}}{2a}\check{\mathbf{e}}_y. \qquad (21c)$$

For the fixed points quadratic polynomial (20), $a = 1, b = -1$. From (21a)-(21c), the solutions (19a)-(19c) are obtained. $\qquad\qquad\qquad\qquad\square$

In contrast with the quadratic polynomial in the complex field, where the roots are either both real or both imaginary, the hypercomplex solutions can coexist with the real or complex like solutions in $\mathbb{S}^{1+2}$. We refer to hypercomplex roots to those solutions where the scalar and both director components are different from zero.

- If $-\frac{1}{4} \leq c \leq \frac{1}{4}$, only the usual two, possibly degenerate, real solutions exist. Outside this region, there are additionally four hypercomplex roots.

- For $c < -\frac{1}{4}$, there are six fixed points. In addition to the two real points, there are four fixed points due to the hypercomplex roots. These point lie in the $\check{\mathbf{e}}_x, \check{\mathbf{e}}_y$ plane in the negative $s$ semispace at $s = c + \frac{1}{4}$.

- For $c > \frac{1}{4}$, there are eight fixed points. Four fixed points, two in the $s, \check{\mathbf{e}}_x$ plane and two in the $s, \check{\mathbf{e}}_y$ plane. These points correspond to the usual solutions in the complex plane, but there are now two hypercomplex planes sharing the scalar axis. There is no precedence of the two hyperimaginary axes, the two hyperimaginary units $\check{\mathbf{e}}_x$ or $\check{\mathbf{e}}_y$ become identical to the $i$ imaginary unit if only one (hyperimaginary) director component is present. In addition, there are four hypercomplex roots in the positive $s$ semispace at the $s = c + \frac{1}{4}$ plane. There exist hypercomplex roots ($|4ac| > b^2$) whenever there exist complex like roots ($4ac > b^2$).

The hypercomplex roots have director components with equal absolute value. Therefore, the four fixed points lie symmetrically placed in 45° planes with respect to the $\check{\mathbf{e}}_x, \check{\mathbf{e}}_y$ axes. Just as in the complex plane, the constant $c$ may be any point in $c \in \mathbb{C}$; in $\mathbb{S}^{1+2}$, the constant $\overset{o}{c}$ can be any point in the $\mathbb{S}^{1+2}$ scator set. However, analytic solutions to the quadratic equation in $\mathbb{S}^{1+2}$ are only available at present for scalar (real) $\overset{o}{c}$.

*4.1.  $c = -\frac{1}{2}$, connected set*

If $\overset{o}{c} = -\frac{1}{2} + 0\,\check{\mathbf{e}}_x + 0\,\check{\mathbf{e}}_y$, from (19b) the well known two real roots are obtained. These two fixed points $\overset{o}{\varphi}_{\mathbb{S}^{1+0}} = \frac{1}{2} \pm \frac{\sqrt{3}}{2}$, are shown in red in the complex plane 2D rendering in figure 6a. As usual, one of them is at the boundary $\overset{o}{\varphi}_{\mathbb{S}^{1+0},+} = \frac{1}{2} + \frac{\sqrt{3}}{2} \in J\big(\overset{o}{\varphi}^2 - \frac{1}{2}\big)$, while the other is an interior point $\overset{o}{\varphi}_{\mathbb{S}^{1+0},-} = \frac{1}{2} - \frac{\sqrt{3}}{2} \in$
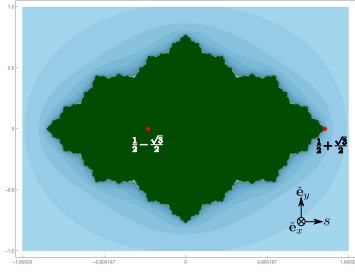
(a) Julia set for $c = -\frac{1}{2}$. Fixed points in the real axis shown in red.
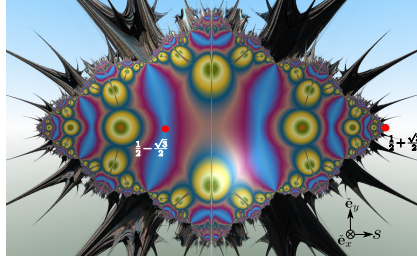


(b) 3D rendering of the $K\!\left(\overset{o}{\varphi}^2 - \frac{1}{2}\right)$ seen from $\overset{o}{\nu}_{obs} = 0 - 2\,\check{\mathbf{e}}_x + 0\,\check{\mathbf{e}}_y$, restricted to $0 \le x \le 10$
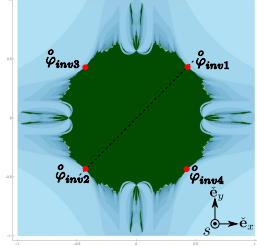






(c) 2D rendering of the $K\!\left(\overset{o}{\varphi}^2 - \frac{1}{2}\right)$, $s = -0.25$. The fixed hypercomplex points are shown in red.
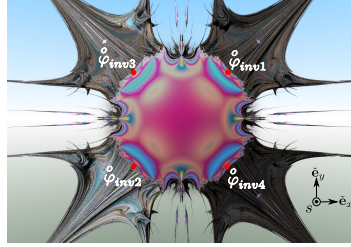
(d) 3D rendering of the $K\!\left(\overset{o}{\varphi}^2 - \frac{1}{2}\right)$ seen from $\overset{o}{\varphi}_{obs} = 2 + 0\,\check{\mathbf{e}}_x + 0\,\check{\mathbf{e}}_y$, restricted to $-10 \le x \le -0.25$
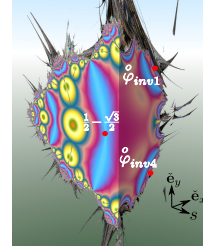
(e) $K\!\left(\overset{o}{\varphi}^2 - \frac{1}{2}\right)$, restricted to $-10 \le s \le -0.25$ and $0 \le x \le 10$.

Figure 6: Non divergent set in $\mathbb{S}^{1+2}$ dynamic space for $c = -\frac{1}{2}$.

$K\big(\overset{o}{\varphi}^2 - \tfrac{1}{2}\big) \setminus J$. This set is also shown in a 3D rendering in figure 6b. The $K\big(\overset{o}{\varphi}^2 - \tfrac{1}{2}\big)$ volume has been restricted to the positive semi-space, thus exhibiting the $x = 0$ plane in the forefront since the viewpoint is located on the $\check{\mathbf{e}}_x$ axis at $-2$, i.e. $\overset{o}{v}_{obs} = 0 - 2\,\check{\mathbf{e}}_x + 0\,\check{\mathbf{e}}_y$.

In addition to these two real roots, the hypercomplex roots from (19a) are

$$\overset{o}{\varphi}_{\mathbb{S}^{1+2}\setminus\mathbb{S}^{1+1}} = -\frac{1}{4} \pm \frac{\sqrt{3}}{4}\check{\mathbf{e}}_x \pm \frac{\sqrt{3}}{4}\check{\mathbf{e}}_y. \tag{22}$$

These invariant points, labeled $\overset{o}{\varphi}_{inv1}$ to $\overset{o}{\varphi}_{inv4}$ for the $++, --, -+, +-$ sign combintations respectively, are shown in red in figure 6c; where a two dimensional rendering of the $K\big(\overset{o}{\varphi}^2 - \tfrac{1}{2}\big)$ volume intersection with the $\check{\mathbf{e}}_x, \check{\mathbf{e}}_y$ plane at $s = -0.25$ is depicted. These four hypercomplex roots seem to belong to the $J$ set since they visually lie on the boundary of the filled in set, $J\big(\overset{o}{\varphi}^2 - \tfrac{1}{2}\big) = \partial K\big(\overset{o}{\varphi}^2 - \tfrac{1}{2}\big)$. This set is the higher dimensional analogue of the Julia set in the complex plane. In figure 6d, a 3D rendering is shown viewed from the $s$ axis, the $K\big(\overset{o}{\varphi}^2 - \tfrac{1}{2}\big)$ set is limited to the interval $-0.25 \geq s \geq -10$. A perspective where two of the hypercomplex fixed points and one of the real fixed points are shown in red, is depicted in figure 6e. There are then 6 forward invariant points in the $K\big(\overset{o}{\varphi}^2 - \tfrac{1}{2}\big)$ set in $\mathbb{S}^{1+2}$ scator space, in contrast with the 2 fixed points in $\mathbb{S}^{1+1}$ scator space (equivalent to the complex plane).

## 5. Inverse orbits

Recall that the Julia set $J(f) = \partial K(f)$ is the closure of the set of repelling periodic points. If the function is inverted, the set of limit points of the iterated backward orbits gives the Julia set.

**Lemma 5.1.** *The inverse orbits of the quadratic function $\overset{o}{f} = \overset{o}{\varphi}^2 + \overset{o}{c}$ where $\overset{o}{f} = s + x\,\check{\mathbf{e}}_x + y\,\check{\mathbf{e}}_y$ and $\overset{o}{c} = c_s + c_x\,\check{\mathbf{e}}_x + c_y\,\check{\mathbf{e}}_y$, are given by*

$$\overset{o}{\zeta}_{\pm,0} = \pm\frac{1}{2}\sqrt{\frac{1}{|s|}}\left(\sqrt{sx_+\,sy_+} + \mathrm{Sgn}x\sqrt{sx_-\,sy_+}\,\check{\mathbf{e}}_x + \mathrm{Sgn}y\sqrt{sx_+\,sy_-}\,\check{\mathbf{e}}_y\right), \tag{23a}$$

*and,*

$$\overset{o}{\zeta}_{\pm,1} = \pm\frac{1}{2}\sqrt{\frac{1}{|s|}}\left(\mathrm{Sgn}x\,\mathrm{Sgn}y\sqrt{sx_-\,sy_-} - \mathrm{Sgn}y\sqrt{sx_+\,sy_-}\check{\mathbf{e}}_x - \mathrm{Sgn}x\sqrt{sx_-\,sy_+}\check{\mathbf{e}}_y\right),$$
$$\tag{23b}$$

*where*

$$sx_+ = \sqrt{(s-c_s)^2 + (x-c_x)^2} + (s-c_s), \quad sx_- = \sqrt{(s-c_s)^2 + (x-c_x)^2} - (s-c_s),$$

$$sy_+ = \sqrt{(s-c_s)^2 + (y-c_y)^2} + (s-c_s), \quad sy_- = \sqrt{(s-c_s)^2 + (y-c_y)^2} - (s-c_s).$$

*Proof.* The inversion of the quadratic function is $\overset{o}{\varphi} = \sqrt{\overset{o}{f} - \overset{o}{c}}$; if the scator components are subtracted, $\overset{o}{f} - \overset{o}{c} = (s - c_s) + (x - c_x)\,\check{\mathbf{e}}_x + (y - c_y)\,\check{\mathbf{e}}_y$. Eqs. (A.1a) and (A.1b) are then invoked to obtain the square roots (23a) and (23b).
□

This Lemma provides an algorithm for visualizing the Julia set in 1+2D. There are four possible roots, on each backward iteration any one of them can be chosen or evaluated in parallel in suitable computer systems. Starting with arbitrary points in $\mathbb{S}^{1+2}$, points in the Julia set are not actually attained but values converge sufficiently close to the $J$ set in a few iterations for visualization purposes. However, this procedure will not render all the nilpotent points due to Lemma 2.11.

From Lemma 4.1, the fixed points given by the hypercomplex roots of the quadratic equation (20) have equal director coefficients magnitudes, $x^2 = y^2$ in (19a). Furthermore, consider the constant $\overset{o}{c}$ to be restricted to a non vanishing scalar value $\overset{o}{c} = c_s$, that is, $c_x = c_y = 0$. Imposing these conditions, the square roots (23a) are

$$\overset{o}{\zeta}_{\pm,0} = \pm\frac{1}{2}\sqrt{\frac{1}{|s - c_s|}}\left(\sqrt{(s - c_s)^2 + x^2} + (s - c_s) + x\,\check{\mathbf{e}}_x + y\,\check{\mathbf{e}}_y\right), \qquad (24a)$$

and (23b)

$$\overset{o}{\zeta}_{\pm,1} = \pm\frac{1}{2}\sqrt{\frac{1}{|s - c_s|}}\left(\mathrm{Sgn}x\,\mathrm{Sgn}y\left[\sqrt{(s - c_s)^2 + x^2} - (s - c_s)\right] - y\,\check{\mathbf{e}}_x - x\,\check{\mathbf{e}}_y\right),$$
$$(24b)$$

where $x$ and $y$ have been retained in the director coefficients to account for their sign.

### 5.1. *Preimages of the $J\left(\overset{o}{\varphi}{}^{2} - \frac{1}{2}\right)$ fixed points*

The Julia set of a function $f$ is invariant under the mapping of $f$ or its inverse. This assertion implies that any point in the Julia set is mapped onto another point within the set for either a forward or a backward orbit. This mapping is usually chaotic. The hypercomplex fixed points for $\overset{o}{c} = -\frac{1}{2} + 0\,\check{\mathbf{e}}_x + 0\,\check{\mathbf{e}}_y$ are given by (22). The $\sqrt{\overset{o}{\varphi}_{inv1} - \left(-\frac{1}{2}\right)} = \sqrt{\frac{1}{4} + \frac{\sqrt{3}}{4}\check{\mathbf{e}}_x + \frac{\sqrt{3}}{4}\check{\mathbf{e}}_y}$ roots from (24a)-(24b) are then

$$\overset{o}{\zeta}_{\pm,0} = \pm\left(\frac{3}{4} + \frac{\sqrt{3}}{4}\,\check{\mathbf{e}}_x + \frac{\sqrt{3}}{4}\,\check{\mathbf{e}}_y\right), \; \overset{o}{\zeta}_{\pm,1} = \pm\left(\frac{1}{4} - \frac{\sqrt{3}}{4}\,\check{\mathbf{e}}_x - \frac{\sqrt{3}}{4}\,\check{\mathbf{e}}_y\right).$$

From these four roots, the outcome of $\overset{o}{\zeta}_{-,1}$ is again the fixed point $\overset{o}{\varphi}_{inv1}$,

$$\sqrt{\overset{o}{\varphi}_{inv1} - \overset{o}{c}} = \left(\frac{1}{4} + \frac{\sqrt{3}}{4}\,\check{\mathbf{e}}_x + \frac{\sqrt{3}}{4}\,\check{\mathbf{e}}_y\right)^{\frac{1}{2}} = \overset{o}{\zeta}_{-,1} = -\frac{1}{4} + \frac{\sqrt{3}}{4}\,\check{\mathbf{e}}_x + \frac{\sqrt{3}}{4}\,\check{\mathbf{e}}_y = \overset{o}{\varphi}_{inv1}.$$

| $\overset{o}{\zeta}_{+,0}$ | $s$ | $x$ | $y$ |
|---|---|---|---|
| $\overset{o}{\varphi}_{inv1}$ | -0.25 | 0.433013 | 0.433013 |
| $\left(\overset{o}{\varphi}_{inv} - \overset{o}{c}\right)^{\frac{1}{2}}$ | 0.75 | 0.433013 | 0.433013 |
| $\vdots$ | 1.15062 | 0.193649 | 0.193649 |
| | 1.28917 | 0.0753636 | 0.0753636 |
| | 1.33819 | 0.0281712 | 0.0281712 |
| | 1.35588 | 0.0103891 | 0.0103891 |
| | 1.36232 | 0.00381307 | 0.00381307 |
| | $\vdots$ | $\vdots$ | $\vdots$ |
| | $\tfrac{1}{2} + \tfrac{\sqrt{3}}{2} \approx 1.36603\ldots$ | 0 | 0 |

Table 1: Inverse orbit of fixed point $\overset{o}{\varphi}_{inv1}$ evaluated with the $\overset{o}{\zeta}_{+,0}$ = $\tfrac{1}{2}\sqrt{\tfrac{1}{|s+\frac{1}{2}|}} \left( \sqrt{\left(s+\tfrac{1}{2}\right)^2 + x^2} + s + \tfrac{1}{2} + x\,\check{e}_x + y\,\check{e}_y \right)$ root. All points belong to the $J$ set (orange points in Figure 7).

The fixed point $\overset{o}{\varphi}_{inv1}$ is forward invariant (by construction) and backward invariant under the action of $\overset{o}{\zeta}_{-,1}$. However, let us consider the action of the other three roots. The inverse orbit iteration evaluated with the $\overset{o}{\zeta}_{+,0}$ root, seems to converge to a constant scalar component while the director components decrease monotonically, as shown in Table 1. A few iterates (orange points) are depicted in Figure 7, where the intersection of the $K\!\left(\overset{o}{\varphi}^2 - \tfrac{1}{2}\right)$ set with a plane having equal director components is pictured. The sequence seems to converge towards $1.36\ldots + 0\,\check{e}_x + 0\,\check{e}_y$, but interestingly, the value of the real fixed point in the Julia set is $\overset{o}{\varphi}_{\mathbb{S}^{1+0},+} = \tfrac{1}{2} + \tfrac{\sqrt{3}}{2} \approx 1.36603\cdots$. The point labeled 1.366 in figure 7 is the same point depicted in the boundary of Figures 6a and 6b. In these two figures, the plane intersecting $K\!\left(\overset{o}{\varphi}^2 - \tfrac{1}{2}\right)$ is $x = 0$ (or $y = 0$), whereas the intersecting plane is $x = y$ in Figure 7. All the points in the sequence are in the boundary of the $K\!\left(\overset{o}{\varphi}^2 - \tfrac{1}{2}\right)$ set.

Backward iterations of $\overset{o}{\varphi}_{inv1}$ with the $\overset{o}{\zeta}_{+,1}$ root, give values with ever smaller scator coefficients in all three components as can be seen in Table 2. While the scalar component decreases monotonically, the director components alternate signs although their absolute value also decreases monotonically. These iterates are shown with cyan dots in Figure 7, the value of one iterate to the next joined by yellow lines. It is interesting to notice that the magnitude of the elements of the sequence seems to converge to $\tfrac{1}{\sqrt{2}}$, after 25 iterations it is $\left\|\overset{o}{\varphi}\right\| = 0.707107$. While the origin is seen as an interior point of the $K\!\left(\overset{o}{\varphi}^2 - \tfrac{1}{2}\right)$ set in the $y = 0$ plane, the indentations of this set in the $x = y$ plane portray the origin as a boundary point. All the points in the sequence again lie in $J = \partial K\!\left(\overset{o}{\varphi}^2 - \tfrac{1}{2}\right)$.
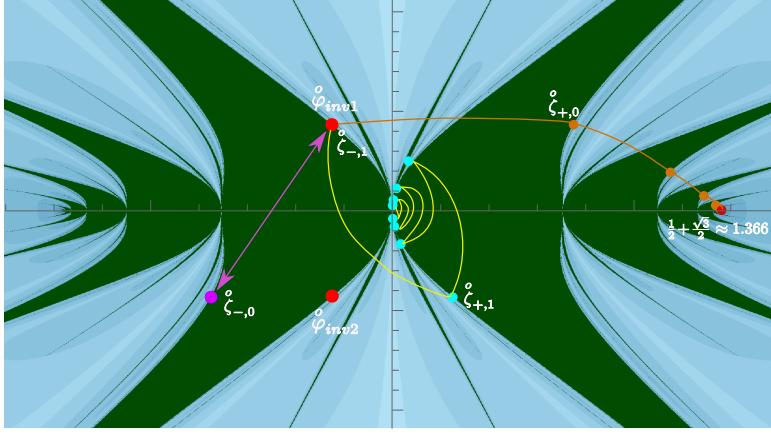
Figure 7: The $K\!\left(\overset{o}{\varphi}{}^{2}-\frac{1}{2}\right)$ set observed at the intersection with the $x=y$ plane (equal director components). The axes plot are $s$ (abscissas) versus $\frac{1}{\sqrt{2}}\left(\check{\mathbf{e}}_x+\check{\mathbf{e}}_y\right)$ (ordinates, shown with a dotted line in Fig. 6c). Inverse orbits of the fixed point $\overset{o}{\varphi}_{inv1}=-\frac{1}{4}+\frac{\sqrt{3}}{4}\check{\mathbf{e}}_x+\frac{\sqrt{3}}{4}\check{\mathbf{e}}_y$ are shown. All the points lie in the boundary of the filled in set, namely in the $\partial K\!\left(\overset{o}{\varphi}{}^{2}-\frac{1}{2}\right)=J$ set.

| $\overset{o}{\zeta}_{+,1}$ | $s$ | $x$ | $y$ | $\left\lVert\overset{o}{\varphi}\right\rVert$ |
|---|---|---|---|---|
| $\overset{o}{\varphi}_{inv1}$ | -0.25 | 0.433013 | 0.433013 | 1 |
| $\left(\overset{o}{\varphi}_{inv1}-\overset{o}{c}\right)^{\frac{1}{2}}$ | 0.25 | -0.433013 | -0.433013 | 1 |
| $\vdots$ | 0.0669873 | 0.25 | 0.25 | 1 |
|  | 0.0349738 | -0.166006 | -0.166006 | 0.823 |
|  | 0.0172025 | 0.113482 | 0.113482 | 0.766 |
|  | 0.00855398 | -0.0788981 | -0.0788981 | 0.736 |
|  | 0.00426558 | 0.0553182 | 0.0553182 | 0.722 |
|  | 0.00213004 | -0.0389501 | -0.0389501 | 0.714 |
|  | 0.00106434 | 0.0274834 | 0.0274834 | 0.711 |
|  | $\vdots$ | $\vdots$ | $\vdots$ | |

Table 2: Inverse orbit of fixed point $\overset{o}{\varphi}_{inv1}$ evaluated with the $\overset{o}{\zeta}_{+,1}=\frac{1}{2}\sqrt{\frac{1}{\left|s+\frac{1}{2}\right|}}\left(\mathrm{Sgn}x\,\mathrm{Sgn}y\left(\sqrt{\left(s+\frac{1}{2}\right)^{2}+x^{2}}-\left(s+\frac{1}{2}\right)\right)-y\,\check{\mathbf{e}}_x-x\,\check{\mathbf{e}}_y\right)$ root. Magnitude converges to $\frac{1}{\sqrt{2}}\approx 0.707107$.

Finally, backward iterations of $\overset{o}{\varphi}_{inv1}$ with $\overset{o}{\zeta}_{-,0} = -\frac{1}{2}\sqrt{\frac{1}{|s+\frac{1}{2}|}}\left(\sqrt{\left(s+\frac{1}{2}\right)^2 + x^2} + s + \frac{1}{2} + x\,\check{\mathbf{e}}_x + y\,\check{\mathbf{e}}_y\right)$ produce a period two backward orbit alternating between the points

$$-\frac{1}{4} + \frac{\sqrt{3}}{4}\check{\mathbf{e}}_x + \frac{\sqrt{3}}{4}\check{\mathbf{e}}_y \longleftrightarrow -\frac{3}{4} - \frac{\sqrt{3}}{4}\check{\mathbf{e}}_x - \frac{\sqrt{3}}{4}\check{\mathbf{e}}_y.$$

The $\overset{o}{\varphi}_p = -\frac{3}{4} - \frac{\sqrt{3}}{4}\check{\mathbf{e}}_x - \frac{\sqrt{3}}{4}\check{\mathbf{e}}_y$ point is shown in magenta in Figure 7. Since the $J$ set is invariant under the iteration, points in the $J$ set must map to points within the $J$ set. We have not proved that the fixed hypercomplex points belong to the $J$ set. This hypothesis is supported by the visual position of these points in regions that seem to be on the boundary of the $K$ set. All the points shown in Figure 7 again seem to lie on the $\partial K = J$ boundary. Many other cases that are not reported also follow this pattern.

It is not mandatory to use the same root in the backward evaluation of orbits. We could proceed as in some inverse Julia calculations in $\mathbb{C}$, where one of the two roots is randomly chosen. The random choice of one of the four hypercomplex roots in the present case, would fill in many other regions of the $K\left(\overset{o}{\varphi}^2 - \frac{1}{2}\right)$ set intersection with the $x = y$ plane (Figure 7). Notice that both, the forward or backward iterations maintain the equality between director coefficients, so that all the iterated points originated from the hypercomplex roots must lie on this plane or its orthogonal version, $x = -y$.

Several interesting cases arise when applying different roots in the inverse orbit calculations. Let us undertake just one of them as a curious example. Consider the point $\overset{o}{\varphi}_p = -\frac{3}{4} - \frac{\sqrt{3}}{4}\check{\mathbf{e}}_x - \frac{\sqrt{3}}{4}\check{\mathbf{e}}_y$ that is the partner of the fixed point $\overset{o}{\varphi}_{inv1}$ in the period two backward orbit with the $\overset{o}{\zeta}_{-,0}$ root. If the point $\overset{o}{\varphi}_p$ is backward iterated with the $\overset{o}{\zeta}_{-,1}$ root instead, the result is again $\overset{o}{\varphi}_p$. The point $\overset{o}{\varphi}_p$ is then backwards invariant under $\overset{o}{\zeta}_{-,1}$! However it is not forward invariant, since the forward iteration maps it onto $\overset{o}{\varphi}_{inv1}$.

## 6. Self similarity

Self similarity at arbitrarily small scales is a hallmark of fractal structures. In the Ix-set ($\mathbb{S}^{1+2}$ higher dimensional version of the M-set), we have seen that the main structure is repeated in similar smaller structures. In dynamic space, self-similarity in the complex plane often reproduces the form of the boundary or certain features at different scales rather than the whole object. Self similarity has been observed in many regions of the three dimensional quadratic fractal boundary for a wide variety of $\overset{o}{c}$ values. It is difficult to visualize this feature on the fractal surface due to its intrinsic 'rough' fractal nature. It is sometimes advantageous to limit the fractal rendering to a region in order to visualize the fractal cross section. These cross sections have an altogether different texture and colour, thereby producing much higher contrast. At present we are limited by the software to cross section renderings in planes parallel to the axes. Self

(a) Viewpoint $\overset{o}{v} = 2 + 0\check{\mathbf{e}}_x + 0\check{\mathbf{e}}_y.$ (b) Detail of lower left branch. (c) Further magnification within this branch.

Figure 8: Self similarity of the $K\!\left(\overset{o}{\varphi}^2 - 1\right)$ set. The $\check{\mathbf{e}}_x, \check{\mathbf{e}}_y$ plane is seen from the $s$ axis with $s \leq 0.6$. The cross shaped patterns on the $s = 0.6$ plane keep on repeating at different scales.
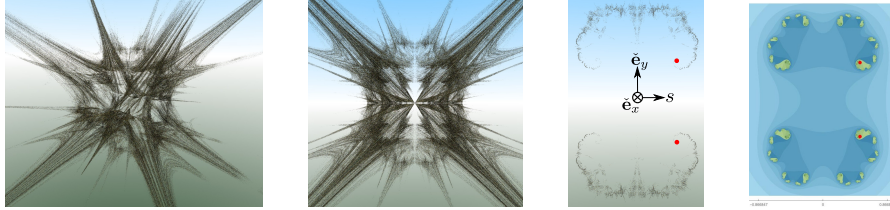


(a) $J\!\left(\overset{o}{\varphi}^2 + \frac{1}{2}\right)$ set seen from $2 - 4\check{\mathbf{e}}_x + 1\check{\mathbf{e}}_y$

(b) $J\!\left(\overset{o}{\varphi}^2 + \frac{1}{2}\right)$ set seen from $0 - 4\check{\mathbf{e}}_x + 0\check{\mathbf{e}}_y$

(c) $J\!\left(\overset{o}{\varphi}^2 + \frac{1}{2}\right)$ set seen from $0 - 3\check{\mathbf{e}}_x + 0\check{\mathbf{e}}_y$, limited to $0 \leq x \leq 0.03$

(d) Julia set for $c = \frac{1}{2}$. Roots at $\frac{1}{2} \pm \frac{1}{2}i$.

Figure 9: Visualization of the non divergent $J$ set of the function $\overset{o}{\varphi}^2 + c$, with $c = \frac{1}{2}$.

similarity of the $K$ set in $\mathbb{S}^{1+2}$ in a region near to the scalar axis and one hyperimaginary plane is perhaps expected because such a plane is close to the complex plane. For this reason, we have chosen to exhibit self similarity in a hyperimaginary-hyperimaginary plane region in Figure 8. The constant has been set at minus one, $\overset{o}{c} = -1 + 0\,\check{\mathbf{e}}_x + 0\,\check{\mathbf{e}}_y$. The part of the set shown in brown streaks is the surface of the volume between $-10 \leq s < 0.6$. The white-yellow-orange cross like features correspond to the $s = 0.6$ plane, where the rendering of the set was stopped. The cross like motives are repeated along the diagonals with different sizes. The brown fibers intertwinings are also repeated again and again but are more difficult to discern. Two close ups shown in Figure 8, keep on revealing more and more crossed motives at different scales.
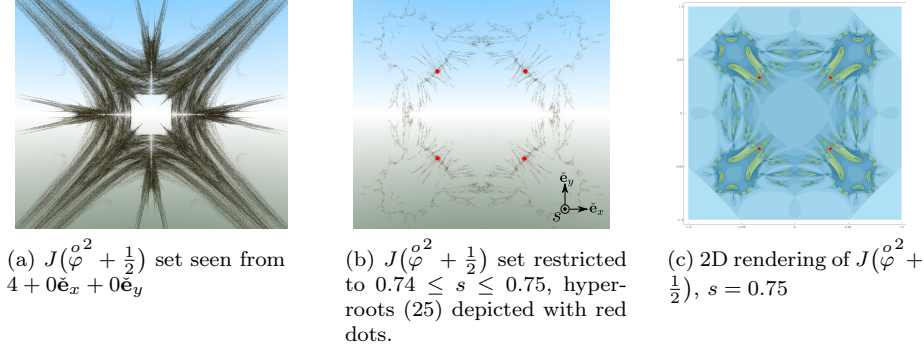
(a) $J\!\left(\overset{o}{\varphi}^{2} + \tfrac{1}{2}\right)$ set seen from $4 + 0\check{\mathbf{e}}_x + 0\check{\mathbf{e}}_y$

(b) $J\!\left(\overset{o}{\varphi}^{2} + \tfrac{1}{2}\right)$ set restricted to $0.74 \leq s \leq 0.75$, hyper-roots (25) depicted with red dots.

(c) 2D rendering of $J\!\left(\overset{o}{\varphi}^{2} + \tfrac{1}{2}\right)$, $s = 0.75$

Figure 10: Visualization of the non divergent set in dynamic space of the function $\overset{o}{f} = \overset{o}{\varphi}^{2} + \tfrac{1}{2}$ seen from the $s$ axis.

## 7. The $c = \tfrac{1}{2}$, non connected set

Consider the non divergent set in dynamic space for the constant $\overset{o}{c} = \tfrac{1}{2} + 0\,\check{\mathbf{e}}_x + 0\,\check{\mathbf{e}}_y$. The 3D rendering, shown in figure 9a, reveals a grainy structure in contrast with the continuous rough surface of the previous examples. A Fatou dust like disconnected set in three dimensions is appreciated. Although there are some more or less dense regions, it is possible to 'see through' in any one of them. If $c = \tfrac{1}{2}$, recall that in $\mathbb{C}$, the Julia set is not connected since $\tfrac{1}{2}$ is not in the M-set. The 3D rendering suggests that, in a similar fashion, since $\tfrac{1}{2}$ is not in the Ix-set, the $J$ set in $\mathbb{S}^{1+2}$ is not connected. This remark will be discussed in more detail in section 8. Let us consider the well known $z = \tfrac{1}{2} \pm \tfrac{1}{2}i$ two fixed points in $\mathbb{C}$ to begin with; they are depicted in red in figure 9d. In $\mathbb{S}^{1+2}$, the corresponding two copies of these roots in the $s, \check{\mathbf{e}}_x$ and $s, \check{\mathbf{e}}_y$ planes are given by (19c), $\overset{o}{\varphi}_{\mathbb{S}^{1+1}_x} = \tfrac{1}{2} \pm \tfrac{1}{2}\check{\mathbf{e}}_x$ and $\overset{o}{\varphi}_{\mathbb{S}^{1+1}_y} = \tfrac{1}{2} \pm \tfrac{1}{2}\check{\mathbf{e}}_y$. These last two roots are depicted in figure 9c. 3D renderings limited to thin regions are particularly difficult to visualize for non connected sets. In this example, if $x$ is restricted to a 0.01 layer or less, there are hardly any points in the plot. As the thickness is increased, more bound points are present but the figure is increasingly less similar to a 2D rendering. A compromise has been chosen, where the layer has been restricted to $0 \leq x \leq 0.03$, in order to evince the similarities of the 3D and 2D mappings in figure 9c and the familiar 2D Julia set shown in figure 9d.

In addition to the two copies of the complex like roots, there are four hyper-complex roots. From (19a),

$$\overset{o}{\varphi}_{\mathbb{S}^{1+2}\setminus\mathbb{S}^{1+1}} = \frac{3}{4} \pm \frac{\sqrt{3}}{4}\check{\mathbf{e}}_x \pm \frac{\sqrt{3}}{4}\check{\mathbf{e}}_y. \qquad (25)$$

These four fixed points are shown in red in the 2D plot in figure 10c. The 3D rendering of the $K\!\left(\overset{o}{\varphi}^{2} + \tfrac{1}{2}\right)$ set, seen straight from the $s$ axis, is shown in figure 10a. The same viewpoint (slightly magnified), but restricted to a thin layer

$0.74 \leq s \leq 0.75$, gives the image shown in 10b. It is finally this last image that resembles the 2D rendering 10c in the hyperimaginary - hyperimaginary plane.

## 8. Conjectures

Differentiability is a necessary condition for a scator function $\overset{o}{\varphi}(\overset{o}{\zeta}) = f_0 + f_x \check{\mathbf{e}}_x + f_y \check{\mathbf{e}}_y$ to be holomorphic. According to a differential quotient criterion, necessary conditions for a function to be differentiable are [19]:

**Theorem 8.1** (Fernandez-Guasti, 2018). *If a scator function $\overset{o}{\varphi} : U \subseteq \mathbb{S}^{1+2} \to \mathbb{S}^{1+2}$ of scator variable $\overset{o}{\zeta}$ in $U \subseteq \mathbb{S}^{1+2}$, is differentiable at the point $\overset{o}{\zeta}_p = z_{0p} + z_{xp}\check{\mathbf{e}}_x + z_{yp}\check{\mathbf{e}}_y$, then the scalar part of the function $f_0$ and the director parts of the function $f_x, f_y$, are real differentiable $C^1$ functions that satisfy the partial differential equations*

$$\frac{\partial f_0}{\partial z_0} = \frac{\partial f_x}{\partial z_x} = \frac{\partial f_y}{\partial z_y}, \tag{26a}$$

$$\frac{\partial f_x}{\partial z_0} = -\frac{\partial f_0}{\partial z_x}, \quad \frac{\partial f_y}{\partial z_0} = -\frac{\partial f_0}{\partial z_y} \tag{26b}$$

$$\frac{\partial f_0}{\partial z_x}\frac{\partial f_0}{\partial z_y} = -\frac{\partial f_x}{\partial z_x}\frac{\partial f_x}{\partial z_y}, \tag{26c}$$

*evaluated at the point $\overset{o}{\zeta}_p$.*

The partial derivatives involved in (26a) and (26b), resemble the Cauchy-Riemann conditions extended to a real and two hyperimaginary dimensions. The square function does not satisfy conditions (26a), (26b) and (26c). Therefore, the square function is not holomorphic anywhere in the scator set. However, it is scator differentiable for points $\overset{o}{\zeta}_p$ with $y = 0$, or $x = 0$ since then all crossed terms are equal to zero. This result is expected because the $s + x\,\check{\mathbf{e}}_x + 0\,\check{\mathbf{e}}_y$ or the $s + 0\,\check{\mathbf{e}}_x + y\,\check{\mathbf{e}}_y$ planes are identical to the complex plane where the square function is complex holomorphic. The lack of holomorphy according to a differential quotient criterion of the square function prevents us from evaluating its derivatives and their subsequent computation at the critical points. Thus, the classical fractal classification of points into super-attractive, attractive, indifferent or repelling, depending on the value of its derivative, cannot be readily performed for the quadratic mapping in the $\mathbb{S}^{1+2}$ scator realm. Furthermore, in $\mathbb{S}^{1+2}$ it is not possible, according to the differential quotient criterion, to define Fatou or Julia sets in terms of normal meromorphic families, because the scator quadratic function is not meromorphic. The scator holomorphic functions in $\mathbb{S}^{1+2}$ have been divided into three families [20]: the components exponential (cexp) function, linear functions and exceptional solutions. The cexp function holomorphy permits the multiplicative representation of scators. Whereas the exceptional solutions involve single variable arbitrary functions of one variable [20]. The scator holomorphic functions set, according to the differential quotient criterion, is considerably larger than their counterpart in Clifford Algebras.

Nonetheless, an individual investigation of the forward orbits of several tens of points in $\mathbb{S}^{1+2}$ consistently showed the following outcome after 25 iterations: i) For $\overset{o}{c} = -\frac{1}{2}$, all sequences either approached $\overset{o}{\varphi}_{\mathbb{S}^{1+0}} = \frac{1}{2} - \frac{\sqrt{3}}{2} \approx -0.366\cdots$ ($\in K$ set) or become very large $> 10^9$ ($\in F$ set). ii) Points in the $\mathbb{S}^{1+2} \setminus \mathbb{S}^{1+1}$ set converge faster than points in $\mathbb{S}^{1+1}$. To illustrate this latter assertion, the point $1 + 0.3\,\check{\mathbf{e}}_x + 0.2\,\check{\mathbf{e}}_y$ after 25 iterates is equal to $\approx -0.36651 - 4.17 \times 10^{-9}\,\check{\mathbf{e}}_x - 8.74 \times 10^{-4}\,\check{\mathbf{e}}_y$, while the point $1 + 0.3\,\check{\mathbf{e}}_x + 0\,\check{\mathbf{e}}_y$ is equal to $\approx -0.36804 + 9.20 \times 10^{-4}\,\check{\mathbf{e}}_x$ after the same number of iterates. For all the non divergent probed points, the interior fixed point $\frac{1}{2} - \frac{\sqrt{3}}{2}$ plays the role of an attractive point in $\mathbb{S}^{1+2}$, just as it does in the complex domain. The partial directional derivatives of the quadratic function $\overset{o}{\varphi}^2 + \overset{o}{c}$ depending on the direction where from the limit is taken are [19]

$$\frac{\partial}{\partial s}\left(\overset{o}{\varphi}^2 + \overset{o}{c}\right) = 2s\left(1 - \frac{x^2 y^2}{s^4}\right) + 2x\left(1 + \frac{y^2}{s^2}\right)\check{\mathbf{e}}_x + 2y\left(1 + \frac{x^2}{s^2}\right)\check{\mathbf{e}}_y,$$

$$\frac{\partial}{\partial x\,\check{\mathbf{e}}_x}\left(\overset{o}{\varphi}^2 + \overset{o}{c}\right) = 2s\left(1 - \frac{y^2}{s^2}\right) + 2x\left(1 - \frac{y^2}{s^2}\right)\check{\mathbf{e}}_x + 4y\,\check{\mathbf{e}}_y,$$

$$\frac{\partial}{\partial y\,\check{\mathbf{e}}_y}\left(\overset{o}{\varphi}^2 + \overset{o}{c}\right) = 2s\left(1 - \frac{x^2}{s^2}\right) + 4x\,\check{\mathbf{e}}_x + 2y\left(1 - \frac{x^2}{s^2}\right)\check{\mathbf{e}}_y.$$

Recall from Subsec. 2.2 that the multiplicative inverse is $\overset{o}{\varphi}^{-1} = \overset{o}{\varphi}^* \|\overset{o}{\varphi}\|^{-2}$, thus $\frac{1}{\check{\mathbf{e}}_x} = -\check{\mathbf{e}}_x$, $\frac{1}{\check{\mathbf{e}}_y} = -\check{\mathbf{e}}_y$. On the scalar (real) line, $x = y = 0$, all three derivatives are equal to $2s$. The magnitude of the derivative for the fixed point $\overset{o}{\varphi}_{\mathbb{S}^{1+0}} = \frac{1}{2} - \frac{\sqrt{3}}{2}$ is $0 < |1 - \sqrt{3}| < 1$; therefore, it is an attractive point according to the usual classification. Analogous results hold for points in the $s, \check{\mathbf{e}}_x$ or $s, \check{\mathbf{e}}_y$, for the roots $\overset{o}{\varphi}_{\mathbb{S}_x^{1+1}} = \frac{1}{2} \pm \frac{1}{2}\check{\mathbf{e}}_x$ and $\overset{o}{\varphi}_{\mathbb{S}_y^{1+1}} = \frac{1}{2} \pm \frac{1}{2}\check{\mathbf{e}}_y$. Whether this criterion suffices to claim that these points are attractive in $\mathbb{S}^{1+2}$, remains to be seen. For the hypercomplex roots, the partial derivatives are not equal, for example, if $s + x\check{\mathbf{e}}_x + y\check{\mathbf{e}}_y = -\frac{1}{4} \pm \frac{\sqrt{3}}{4}\check{\mathbf{e}}_x \pm \frac{\sqrt{3}}{4}\check{\mathbf{e}}_y$,

$$\frac{\partial}{\partial s}\left(\overset{o}{\varphi}^2 + \overset{o}{c}\right) = 4 \pm 2\sqrt{3}\check{\mathbf{e}}_x \pm 2\sqrt{3}\check{\mathbf{e}}_y, \quad \left\|\frac{\partial}{\partial s}\left(\overset{o}{\varphi}^2 + \overset{o}{c}\right)\right\| = 7.$$

and (an equivalent result holds for $\frac{\partial}{\partial y\check{\mathbf{e}}_y}$)

$$\frac{\partial}{\partial x\check{\mathbf{e}}_x}\left(\overset{o}{\varphi}^2 + \overset{o}{c}\right) = 1 \mp \sqrt{3}\check{\mathbf{e}}_x \pm \sqrt{3}\,\check{\mathbf{e}}_y, \quad \left\|\frac{\partial}{\partial x\check{\mathbf{e}}_x}\left(\overset{o}{\varphi}^2 + \overset{o}{c}\right)\right\| = 4.$$

Although it could be claimed that all three partial directional derivatives satisfy the criterion of repelling points, due to the different values the function is not differentiable at these hypercomplex points.

Many renderings have been performed with different values of the constant $\overset{o}{c}$. In all trials, the $K$ set appears connected if $\overset{o}{c}$ belongs to the Ix-set, the only exception being for large nilpotent points of the form $\overset{o}{\gamma} = \pm g \pm g\check{\mathbf{e}}_x \pm g\check{\mathbf{e}}_y$, with $g$ roughly larger than 2. For $\overset{o}{c}$ values not in the Ix-set, the $J$ set appears like

Cantor dust, some regions more densely populated than others. The $J\!\left(\overset{o}{\varphi}{}^2 + \tfrac{1}{2}\right)$ set, shown in section 7, being representative of this type of sets. If $\overset{o}{c}$ is increased, the Cantor dust is much more thinly populated to the point that it becomes almost indiscernible. From the above discussion together with the numerical evaluation of many $J$ sets, the following two conjectures seem to hold:

Conjecture: The Ix-set, provided that nilpotent points in parameter space are discarded, is the set of parameters where the $J$ set is connected.

Conjecture: The fundamental dichotomy is true in $\mathbb{S}^{1+2}$ scator algebra, the $J$ set is either connected or there exist infinite separate sets.

## 9. Conclusions

Novel two and three dimensional renderings of the quadratic iteration in $\mathbb{S}^{1+2}$ dynamic scator space have been studied and depicted. The sets reveal an intricate fractal boundary that is not easy to visualize due to its complexity. The spikes present for many $\overset{o}{c}$ values, have been described in terms of nilpotent elements at the $m^{th}$ iteration. The $J$ set for the origin has been shown to be equal to the unit isometric cusphere scator surface. Fixed points have been evaluated invoking the solution to the scator quadratic polynomial equation with real coefficients. The number of fixed points is increased due to the existence of four hypercomplex roots if $|4c| > 1$. Some of the main features have been exemplified with two sets, $K\!\left(\overset{o}{\varphi}{}^2 - \tfrac{1}{2}\right)$ and $K\!\left(\overset{o}{\varphi}{}^2 + \tfrac{1}{2}\right)$ that seem to be connected and disconnected respectively. Other parameters are likely to reveal new features of the 3D sets. These two representative examples were chosen on two grounds: Analytical solutions for the fixed points are possible for scalar values of the constant, $\overset{o}{c} = c_s$ (Lemma 4.1). Values of $c_s = \pm\tfrac{1}{2}$ such that $|4c_s| > 1$ have been chosen so that there exist hypercomplex roots. These roots are emergent solutions without a counterpart in the complex set. For these values of $\overset{o}{c}$, the $K$ interior attractive fixed point in $\mathbb{C}$ also acts as the attractive fixed point for the forward orbits in $\mathbb{S}^{1+2}$. The algorithm for evaluating inverse orbits for arbitrary $\overset{o}{c} \in \mathbb{S}^{1+2}$ has been derived (Lemma 5.1). Sets of points very close to $J$ in $\mathbb{S}^{1+2}$ can thus generated from inverse orbits of arbitrary points. Inverse orbits of the hypercomplex fixed points reveal a richer dynamic behaviour compared with their 2D counterpart. An infinite number of points belonging to $J$ in the $x = y$ plane can be generated with this procedure. Sets in dynamic space exhibit self similar boundary shapes at different scales.It has been conjectured that some of the fundamental fractal theorems in the complex set are also valid in the $\mathbb{S}^{1+2}$ scator set.

### Acknowledgements

## Appendix A. Scator square roots in additive variables

The square roots $\sqrt{\overset{o}{\varphi}} = \sqrt{s + x\,\check{\mathbf{e}}_x + y\,\check{\mathbf{e}}_y}$ of a scator $\overset{o}{\varphi} \in \mathbb{S}^{1+2}$ in the additive representation with additive variables are given by Lemma 4.2 in [14]

$$
\sqrt{\overset{o}{\varphi}} = \overset{o}{\zeta}_{\pm,0} = \pm\frac{1}{2}\sqrt{\frac{1}{|s|}}\left[\sqrt{\left(\sqrt{s^2+x^2}+s\right)\left(\sqrt{s^2+y^2}+s\right)}\right.
$$
$$
+ \operatorname{Sgn}x\sqrt{\left(\sqrt{s^2+x^2}-s\right)\left(\sqrt{s^2+y^2}+s\right)}\,\check{\mathbf{e}}_x
$$
$$
\left. +\operatorname{Sgn}y\sqrt{\left(\sqrt{s^2+x^2}+s\right)\left(\sqrt{s^2+y^2}-s\right)}\,\check{\mathbf{e}}_y\right], \quad (A.1a)
$$

and from the $\pi$-pair symmetry,

$$
\sqrt{\overset{o}{\varphi}} = \overset{o}{\zeta}_{\pm,1} = \pm\frac{1}{2}\sqrt{\frac{1}{|s|}}\left[\operatorname{Sgn}x\,\operatorname{Sgn}y\sqrt{\left(\sqrt{s^2+x^2}-s\right)\left(\sqrt{s^2+y^2}-s\right)}\right.
$$
$$
- \operatorname{Sgn}y\sqrt{\left(\sqrt{s^2+x^2}+s\right)\left(\sqrt{s^2+y^2}-s\right)}\check{\mathbf{e}}_x
$$
$$
\left. -\operatorname{Sgn}x\sqrt{\left(\sqrt{s^2+x^2}-s\right)\left(\sqrt{s^2+y^2}+s\right)}\check{\mathbf{e}}_y\right]. \quad (A.1b)
$$

From these expressions, with the substitutions $s \to (\pm g - c_0)$, $x \to (\pm g - c_x)$, $y \to (\pm g - c_y)$, the coefficients of $\overset{o}{\varphi}_1$ that produce a square nilpotent term on the second iteration are obtained. If $\overset{o}{c} = c_0$, and the director components of this constant are zero, $c_x = c_y = 0$, the roots simplify to (18a) and (18b).

## References

[1] M. Fernández-Guasti, Imaginary scators bound set under the iterated quadratic mapping in 1+2 dimensional parameter space, Int. J. of Bifurcation and Chaos 26 (2016) 1630002.

[2] J. Gomatam, J. Doyle, B. Steves, I. McFarlane, Generalization of the Mandelbrot set: Quaternionic quadratic maps, Chaos, Solitons & Fractals 5 (1995) 971–986.

[3] S. Bedding, K. Briggs, Iteration of quaternion maps, International Journal of Bifurcation and Chaos 05 (1995) 877–881.

[4] J. Cheng, J. R. Tan, Generalization of 3d Mandelbrot and Julia sets, Journal of Zhejiang University - Science A 8 (2007) 134–141.

[5] D. White, P. Nylander, Triplex algebra, http://www.fractalforums.com/theory/triplex-algebra/, 2009.

[6] B. Rama, J. Mishra, Generation of 3D fractal images for Mandelbrot set, in: Proceedings of the 2011 International Conference on Communication, Computing & Security, ICCCS '11, ACM, New York, NY, USA, 2011, pp. 235–238.

[7] P. Bonzini, To quaternions and back, http://www.fractal.org/mbulb-paolo-bonzini.pdf, 2010.

[8] Y. Araki, Materializing 3d quasi-fuchsian fractals, Forma 21 (2006) 19–27.

[9] J. Aron, The mandelbulb: first 'true' 3d image of famous fractal, New Scientist 204 (2009) 54.

[10] K. Sanderson, 2009 gallery: Images of the year, Nature 462 (2009) 972–977.

[11] I. L. Kantor, A. S. Solodovnikov, Hypercomplex numbers, Springer-Verlag, 1989. Translated by A. Shenitzer.

[12] M. Fernández-Guasti, Powers of elliptic scator numbers, Axioms 10 (2021) 250.

[13] M. Fernández-Guasti, Roots of elliptic scator numbers, Axioms 10 (2021) 321.

[14] M. Fernández-Guasti, Multiplicity of scator roots and the square roots in $S^{1+2}$, J. New Theory 42 (2023) 43–56.

[15] M. Fernández-Guasti, Roots of second order polynomials with real coefficients in elliptic scator algebra, J. New Theory 36 (2021) 39–48.

[16] M. Fernández-Guasti, F. Zaldívar, An elliptic non distributive algebra, Adv. Appl. Clifford Algebras 23 (2013) 825–835.

[17] M. Fernández-Guasti, Associativity in scator algebra and the quantum wavefunction collapse, Universal Journal of Mathematics and Applications 1 (2018) 80–88.

[18] M. Fernández-Guasti, The cusphere, Mathematics and the Arts (2023). in print.

[19] M. Fernández-Guasti, Differential quotients in elliptic scator algebra, Math. Meth. App. Sci. 41 (2018) 4827–4840.

[20] J. L. Cieśliński, D. Zhalukevich, Explicit formulas for all scator holomorphic functions in the (1+2)-dimensional case, Symmetry 12 (2020) 1550.